Ore Geology Reviews 143 (2022) 104779

Contents lists available at ScienceDirect

Ore Geology Reviews

journal homepage: www.elsevier.com/locate/oregeorev

Nb/Ta, Zr/Hf and REE fractionation in exotic pegmatite from the Keivy province, NW Russia, with implications for rare-metal mineralization in alkali feldspar granite systems

Dmitry Zozulya [a,*], Ray Macdonald [b,c], Bogusław Bagiński [b], Petras Jokubauskas [b]

[a] Geological Institute, Kola Science Centre, 14 Fersman Str, 184209 Apatity, Russia
[b] Department of Geochemistry, Mineralogy and Petrology, Faculty of Geology, University of Warsaw, al. Żwirki i Wigury 93, 02-089 Warsaw, Poland
[c] Environment Centre, Lancaster University, Lancaster LA1 4YQ, UK

ARTICLE INFO

Keywords:
Astrophyllite
Titanite
Ferriallanite
Pegmatite
Alkali feldspar granite
REE, Nb/Ta, Zr/Hf fractionation
Rare-metal deposits
Keivy
NW Russia

ABSTRACT

The White Tundra pegmatites are associated with the Keivy alkali feldspar granite complex in the Kola Peninsula, NW Russia. The host granites are aegirine-arfvedsonite, biotite-arfvedsonite and biotite-ferrohastingsite varieties, ranging compositionally from peralkaline through metaluminous to peraluminous. The pegmatites are remarkable for the diversity of the rare-metal mineralization. The inferred crystallization sequence of the main REE, HFSE and Ti minerals in the pegmatite is: zircon – fergusonite-(Y) – monazite-(Ce) – gadolinite-hingganite series – britholite-(Y) – astrophyllite – titanite – allanite-(Ce) — chevkinite-(Ce) – ilmenite – kainosite-(Y) – REE carbonates. The pegmatites show unusual parageneses indicating a transition of the mineral associations from agpaitic to miaskitic in the same body (e.g. zirconosilicate → zircon; astrophyllite → titanite). A number of minerals have anomalous minor element contents. Astrophyllite and some titanites have low (even < 1) Nb/Ta and Zr/Hf ratios that contrast with the overall geochemical environment (ratios ≫ 1); titanite with very high Y and HREE contents; elevated Sn, W and V contents in some titanosilicates; allanite-(Ce) with very high Ti contents coupled with low (less than stoichiometric) values of Al, suggesting a Ti → Al substitution. Whole-rock compositions of the host granite show a steady decrease of Nb/Ta and Zr/Hf ratios in peralkaline through metaluminous to peraluminous types. Compositions of Ti minerals suggest that further fractionation of Nb-Ta, Zr-Hf and REE in the White Tundra exotic pegmatite and the crystallization of Ti minerals with anomalous compositions are due to a combination of several factors: assimilation by the primary magma (enriched in Zr, Nb, REE) of upper crustal lithologies enriched in Ta, Hf, LREE, W, Sn; consumption of significant amounts of Nb and Zr by early-crystallized pegmatitic fergusonite and zircon with Nb/Ta and Zr/Hf ≫ 1; transition of HFSE mineral assemblages in pegmatite from agpaitic to miaskitic with consequent lowering of Nb/Ta and Zr/Hf; crystallization of minerals in a low-temperature (hydrothermal) environment with changing F contents, that promoted a sporadic further decrease of Nb/Ta and Zr/Hf (to values < 1) and increase of Y + HREE. The implications of the fractionation mechanisms for ore-forming processes related to rare-metal granites are discussed.

1. Introduction

Determining the crystallization conditions of pegmatites is very complex because the compositional variations they show are influenced by crystal-melt interactions and melt-crystal-fluid interactions (late magmatic/hydrothermal stages). The pegmatite on which this study focuses, the White Tundra pegmatite, is particularly complex because it comprises five mineralogically different zones and shows evidence of intense mineralization. Previous studies have used zircon (Lyalina et al., 2012), britholite-group minerals (Zozulya et al., 2019) and fergusonite-(Y) (Zozulya et al., 2020) to provide evidence on the composition of the fluids operative at each stage of the pegmatite's development. Here we complement these studies by providing information on the mineral associations, textures and compositions of the Ti-bearing silicates astrophyllite, titanite and Ti-rich allanite. A particular value of these minerals is that they can be used to examine the fractionation of three sets of coherent or "twin" elements, Nb from Ta, Zr from Hf, and within the rare-earth elements (REE), which has been shown to provide insights

* Corresponding author.
E-mail address: zozulya@geoksc.apatity.ru (D. Zozulya).

https://doi.org/10.1016/j.oregeorev.2022.104779
Received 21 September 2021; Received in revised form 9 February 2022; Accepted 12 February 2022
Available online 15 February 2022

into the processes operating in evolved melts and in the formation of rare-metal ores.

The fractionation may be the result of a number of processes (Boily and Williams-Jones, 1994; Linnen et al., 2014; Stepanov et al., 2014; Breiter and Škoda, 2017; Li et al., 2017; Ballouard et al., 2020). It most commonly occurs during the magmatic stages by fractional crystallization, due to the different compatibilities between solid phases and melt for individual REE, Nb and Ta, and Zr and Hf. An example is the increase in LREE/HREE ratios in residual melts. It can also be controlled by crystallochemical factors, including different rates of incorporation of trace elements into the rock-forming minerals, such as the preferential incorporation of Nb into micas, amphibole and ilmenite, while subsequent fractionation of these minerals decreases Nb/Ta ratios in the melt.

REE, Nb-Ta and Zr-Hf fractionation also occurs during postmagmatic processes; however, they are less fully studied due to the great diversity and complexity of the parageneses, such as the different geochemical environments and physicochemical conditions, the different complexity of metals, changes of fluid-and-solution compositions, and the multistage character of the alteration. A commonly observed feature is an increase in the HREE/LREE ratios during the hydrothermal stage(s) (Kosterin, 1959; Mineev, 1963, 1968; Taylor et al., 1981; Charoy and Raimbault, 1994). Some experiments have shown that Ta appears to be less soluble than Nb (e.g., Zaraisky et al., 2010). Therefore, Nb will tend to be carried away preferentially by fluids, resulting in a decrease of the whole-rock Nb/Ta ratios. An increase in the Hf content in zircon with a temperature drop during the hydrothermal stages is often observed (Hanchar and Hoskin, 2003; Wang et al., 2010; Lyalina et al., 2012; Breiter and Škoda, 2017).

Variations in whole-rock Nb/Ta and Zr/Hf ratios are well documented for alkaline and subalkaline rock series. Nb/Ta ratios in oversaturated and undersaturated alkaline rocks are equal to, and often higher than, ocean island and intraplate continental basalt values (~15–20), whereas Nb/Ta ratios in subalkaline rocks are lower, reaching 0–5 in peraluminous granites (Ballouard et al., 2020, and references therein). Zr/Hf ratios are near-chondritic (35–40) in most magmatic rocks while highly evolved, high-silica rocks have anomalously low Zr/Hf (15–30) (Lowery Claiborne et al., 2006).

Rocks termed agpaitic contain complex Na–K–Ca–Fe bearing silicates enriched in Nb, Ti, Zr and REE (e.g. eudialyte, aenigmatite, astrophyllite, catapleiite, elpidite, gittinsite, dalyite, rinkite-(Ce); loparite-(Ce)). In contrast, in miaskitic alkaline rocks HFSE and REE are accommodated mainly in zircon, baddeleyite, titanite, allanite, perovskite, and Fe–Ti oxides (ilmenite or Ti-bearing magnetite). The nature and mechanisms of the transition between the assemblages has been actively debated in recent years (Sørensen, 1997; Marks et al., 2011; Andersen et al., 2016; Marks and Markl, 2017; Chakrabarty et al., 2018). The White Tundra pegmatite contains both types of assemblage (astrophyllite and titanite + allanite), allowing us to comment on the possible agpaitic to miaskitic mineral assemblage transition.

Astrophyllite group minerals are alkali (K, Na), Fe- or Mn- dominant titanosilicates. The Ti site can be substituted by Nb (with trace amounts of Ta (up to 0.13 apfu)) forming extensive solid solution (>80%) with Nb-dominant niobokupletskite and niobophyllite (Piilonen et al., 2003). Substitution of Zr (and trace Hf (up to 0.04 apfu)) for Ti is less extensive (51% solid solution), resulting in zircophyllite. Astrophyllite-group minerals are characteristic of alkaline (both Si-undersaturated and Si-oversaturated) rocks and associated pegmatites and occur as accessory or main rock-forming minerals.

Titanite is a common accessory mineral of igneous rocks and may contain large amounts of Y + REE (up to 0.06 apfu, Deer et al., 1982), Zr (up to 0.1 apfu, Seifert and Kramer, 2003) and Nb (up to 0.175 apfu, Woolley et al., 1992). It can crystallize both as a primary high-T phase in different magmatic environments, and also as a lower-T phase during metamorphism and hydrothermal activity involving different bulk compositions (Nakada, 1991; Gieré, 1992; Tiepolo et al 2002; Broska et al., 2007; Gao et al., 2012; Chen and Zheng, 2015; Kontonikas-Charos et al., 2019; Gros et al., 2020a; Gros et al., 2020b; Słaby et al., 2021). Titanite is more abundant in granitic pegmatites and metasomatic rocks related to alkaline-carbonatite complexes. These minerals may contain extremely high Nb (0.26 – 0.32 apfu), Ta (0.1 – 0.21 apfu) and Zr (0.12–0.3 apfu) (Groat et al., 1985; Černý et al., 1995; Chakhmouradian, 2004; Kropáč et al., 2020).

Allanite, an REE-Th-rich member of the epidote supergroup, is one of the main carriers of REE in magmatic rocks of acid-intermediate composition but mostly it is a characteristic accessory mineral of miaskitic rocks rather than agpaitic types (Petrik et al., 1995; Gieré and Sorensen, 2004; Vlach and Gualda, 2007; Gros et al., 2020a; Gros et al., 2020b; and references therein). Allanite can be regarded as an important mineral in the study of REE fractionation as it may form Ce-, La-, Nd- and Y-dominant species in various geological environments: magmatic, late- and post-magmatic (Armbruster et al., 2006; Orlandi and Pasero, 2006; Škoda et al., 2012; Alekseev et al., 2013; and references therein).

The Ti minerals studied here are essential constituents of peralkaline granites and associated pegmatites and metasomatites, and in related deposits of heavy rare-earth elements (HREE), Y, Nb, Ta, Be, e.g. Thor Lake and Strange Lake in Canada; Bokan Mountain in USA; Khaldzan Buragtay in Mongolia; Katugin and Ulug-Tanzek in Russia (see reviews by Linnen et al., 2005; Linnen et al., 2014; Verplanck et al., 2014; Kalashnikov et al., 2016). Their study provides important information towards our understanding of ore-forming processes.

2. Geological background

The Keivy alkaline province consists of 2.67–2.65 Ga aegirine-arfvedsonite granites comprising six sheet-like massifs a few hundred meters thick and with a total exposure area of ca. 2500 km^2 (Batieva, 1976; Zozulya et al., 2005; Vetrin and Rodionov, 2009; Balagansky et al., 2021). The largest massifs are West Keivy (1200 km^2), Ponoj (700 km^2) and White Tundra (120 km^2). Aegirine-augite-biotite-ferrohastingsite syenogranites occur at the margins of some massifs. The granites intrude the TTG basement of the Central Kola terrane (NE Fennoscandian shield) and acid-intermediate metavolcanics of the Lebyazha Formation of the Keivy complex (Batieva, 1976; Balagansky et al., 2021). Biotite-ferrohastingsite syenite and biotite-aegirine nepheline syenite ca. 10 km^2 intrusions (Sakharjok occurrences) outcrop within the West Keivy massif. Voluminous coeval gabbro-anorthosites are spatially confined to the Keivy alkali feldspar granites. The peralkaline and ferroan character of the Keivy granites and elevated HFSE contents suggest that the Keivy granites are A-type granitoids. To our knowledge this is the one of the earliest occurrences of fertile A-granite magmatism on Earth (Mitrofanov et al., 2000; Zozulya et al., 2005). Mineralized (rare-metal rich) aegirine-magnetite facies occur in the apical parts of some granite massifs, forming bodies up to 1.5 × 4 km in surface area. Numerous pegmatite bodies are confined to the inner and outer apical parts of Keivy alkali feldspar granite intrusions. They are a few tens of meters long and several meters wide, sometimes with schlieren and oval forms. Compositionally pegmatites are subdivided into quartz-microcline and quartz-feldspar-astrophyllite types. Undoubtedly the A-type granites are the source of the pegmatites, which is confirmed by the same age of a pegmatitic zircon, 2.66 Ga (Lyalina et al., 2012). Dozens of rare-metal deposits and ore occurrences are known from the Keivy alkaline province formed by various petrogenetic (late- and post-magmatic) processes, among which Sakharjok Zr-REE (confined to mineralized syenite), Rova Zr-Y-REE-Nb (mineralized granite – pegmatite – quartzolite), El'ozero Nb-Zr-REE-Th (apobasic metasomatite), and Ploskaya Mt HREE-Y-Nb-Ta (amazonite pegmatite) are the most prominent. They are considered to be promising sources of REE, particularly the more valuable HREE + Y, from the Kola Peninsula (Zozulya et al., 2012, 2019; Bagiński et al., 2016; Kalashnikov et al., 2016; Mikhailova et al., 2017).

The White Tundra granite massif forms an elongated body of ca. 30 km × 2–6 km outcrop. In the north (lowest part of the massif) it turns

into biotite-ferrohastingsite syenogranite dykes, interpreted as magma conduits. The granite and syenogranite dykes embedded large patches (from 10 s to 100 s meters) of gneiss and granite of the TTG complex and metasomatically altered them. The White Tundra granite contains rare xenoliths (up to 1 m size) of the underlying host rocks. To the south the massif contacts the Pana layered basic-ultrabasic intrusion. The contact zone is represented by schistose and amphibolitized pyroxenites and gabbronorites, and by mylonitized alkali feldspar granites.

The pegmatite studied here is from the White Tundra massif (Fig. 1). It is elongated (2 × 5 m) and has a quartz-rich core enclosed by a coarse-grained quartz-arfvedsonite (riebeckite) (±feldspar, Fe-rich biotite) rock with abundant (locally up to 30–40 vol%) Zr-Y-REE-Nb-Th-Ti mineralization and finally rimmed by a pegmatoidal biotite-arfvedsonite granite. Lyalina et al. (2014) divided the body into five zones, reflecting its mineralogical diversity: pegmatitic granite; pegmatite, enriched in astrophyllite; pegmatite, enriched in zircon, galena and astrophyllite; zone of secondary Y-REE mineralization (abundant REE carbonates and silicocarbonates); quartz zone (see Fig. 1 in Lyalina et al. (2014). Ti silicates are characteristic of "astrophyllite" and "secondary Y-REE mineralization" zones. The samples studied here come from the zone of secondary Y-REE mineralization. A remarkable feature of the pegmatite is the occurrence of quartz-zircon aggregates forming spherules and rarely elongated linear intergrowths (Voloshin et al., 2005). The mineral paragenesis and distinctive shape of the aggregates point to a pseudomorphic nature. Voloshin et al. (2005) proposed eudialyte as the precursor mineral and elpidite – to – gittinsite (armstrongite) as secondary (transitional) minerals finally replaced by zircon and quartz.

3. Analytical methods

The chemical compositions of minerals were determined using electron microprobe analysis at the Inter-Institute Analytical Complex at the Department of Geochemistry, Mineralogy, and Petrology, University of Warsaw, using a Cameca SXFive FE electron probe microanalyser

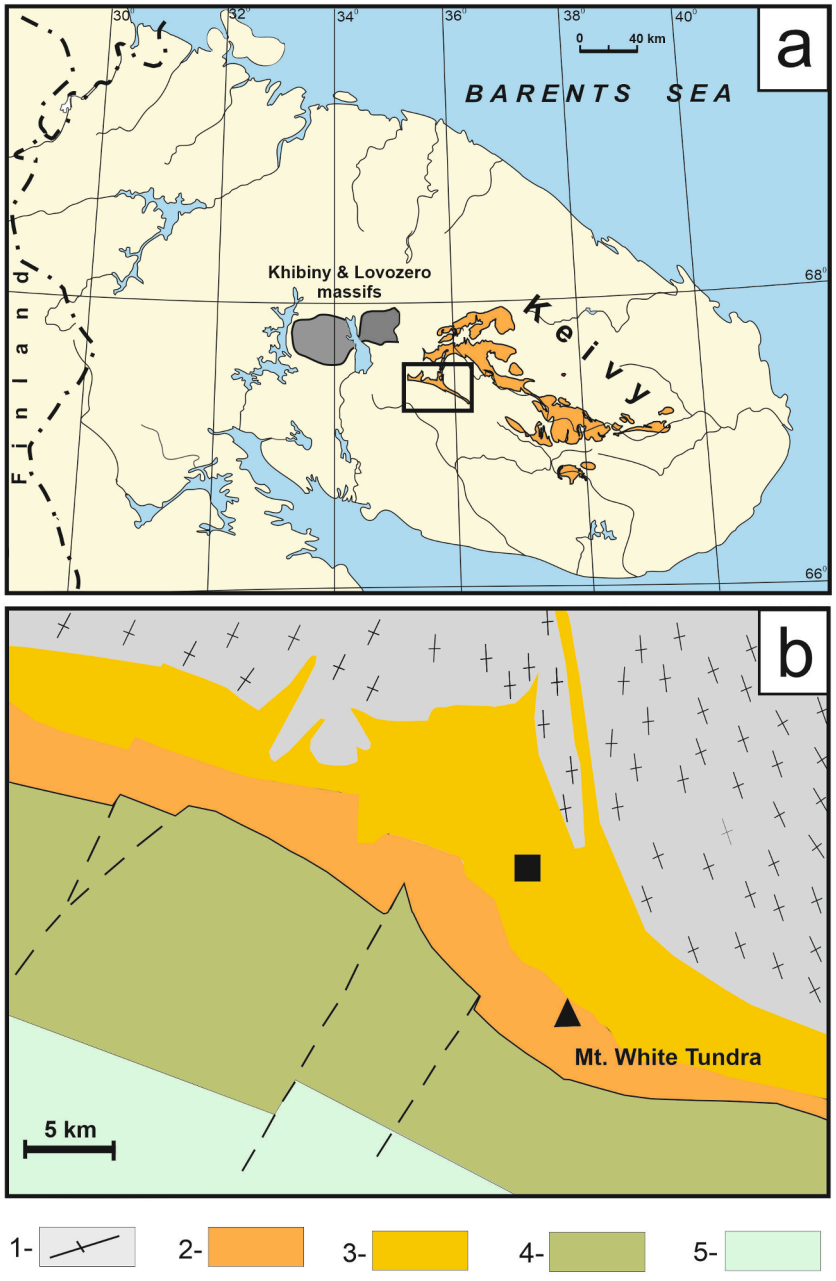

Fig. 1. (a) Location of Keivy alkaline province and (b) geological sketch-map of White Tundra alkali feldspar granite massif (1 – gneiss and granite of TTG complex, AR; 2 – aegirine-arfvedsonite granite, AR2; 3 – biotite-arfvedsonite granite, biotite-hastingsite granite and syenogranite dykes, AR2; 4 – gabbro, PR1; 5- metavolcanics of Imandra-Varzuga belt, PR1). Black square is pegmatite location (coordinates 67.50869:35.76128). Mt White Tundra has coordinates 67.48898:35.77387.

(EPMA), equipped with five wavelength dispersive spectrometers, at the microprobe lab in the Faculty of Geology, University of Warsaw. All measurements were conducted with an electron beam accelerated with 15 kV potential. The beam currents and defocusing of beam were chosen on a point-basis depending on the mineral type and size: 20nA focused beam for astrophyllite, titanite and allanite, 10nA defocused beam for kainosite. Recalculation of X-ray intensities to wt% used the X-PHI (Merlet, 1994) matrix correction model using built-in Cameca absorption coeficients in the Peaksight software. The standards, crystals, and X-ray lines used and the detection limits are given in Supplementary Table S1. Representative electron microprobe data for astrophyllite (14 EPMA analyses), titanite (20 EPMA analyses) and allanite-(Ce) (21 EPMA analyses) were obtained. Additionally associated kainosite (16 EPMA analyses), zircon (37 EPMA analyses) and a hypothetical 'Ca-REE-zirconosilicate' were also analyzed.

Comprehensive element maps of selected areas of interest were made at the Inter-Institute Analytical Complex at the Department of Geochemistry, Mineralogy, and Petrology, University of Warsaw, using a ZEISS SIGMA VP FE (variable pressure, field emission) SEM equipped with an automated stage and two Bruker XFlash 6|10 EDS detectors. The mappings were conducted with an accelerating voltage of 20 kV.

Whole-rock samples of the White Tundra granite were analyzed by wet chemistry methods (oxides, F, Cl) and XRF (Rb, Sr, Y, Nb) in the Geological Institute of the Kola Science Center, Apatity, and by INAA (REE, Zr, Hf, Ta, Th, U) in University of Lowell, Lowell, Massachusetts. Whole-rock samples of the White Tundra granite were analyzed for Nd isotopes in the Laboratory of geochronology and isotope geochemistry of the Geological Institute of the Kola Science Center, Apatity. Measurements of Nd-isotopes and Sm and Nd concentrations were performed by isotope dilution using a Finnigan MAT 262 (RPQ) multicollector mass-spectrometer in a static mode using Ta + Re filaments. The measured reproducibility for two parallel Nd-isotope analyses of the La Jolla standard ($^{143}Nd/^{144}Nd = 0.511833 \pm 6$) was < 0.0024% (2σ). Two $^{147}Sm/^{144}Nd$ measurements of the BCR standard yielded an average error of 0.2% (2σ). Laboratory blanks for Nd and Sm are 0.3 and 0.06 ng, respectively. All $^{143}Nd/^{144}Nd$ ratios were normalized to $^{146}Nd/^{144}Nd = 0.7219$ and corrected using $^{143}Nd/^{144}Nd = 0.511860$ for the concurrent runs of the La Jolla Nd standard.

4. Petrography

4.1. The alkali feldspar granite

The White Tundra alkali feldspar granite is massive, porphyritic with large (1.5–2.0 cm) subhedral phenocrysts of microcline-perthite (40 vol %) and a fine- to medium-grained groundmass composed of equal amounts of xenomorphic albite, quartz, microcline, and schlieren-like segregations of mafic minerals. The morphology of microcline-perthite phenocrysts and albite–oligoclase intergrowths therein, along with the lack of inclusions of late dark-colored minerals, allow us to refer to the microcline-perthite as a primary magmatic mineral. The alkali feldspar granite is leucocratic, the amount of mafic minerals does not exceed 7–8 vol%. The mafic minerals are amphibole ranging from arfvedsonite to hastingsite, aegirine and Fe-rich biotite (±aenigmatite, astrophyllite). Aegirine and aegirine-arfvedsonite varieties tend to occur in the apical part of the massif whereas biotite-arfvedsonite and biotite-hastingsite varieties are in the lower parts (Fig. 1). It is suggested that the latter formed by assimilation of country rocks as they have a hybrid character, notably the occurrence of alkali amphibole and a low (<1) agpaitic index (see below). Ti-silicates are relatively abundant in the White Tundra granite and have distinctive features. Aenigmatite ($Na_2TiFe_5Si_6O_{20}$) and astrophyllite ($K_3Fe_7Ti_2Si_8O_{26}(OH)_5$) are late-magmatic phases in aegirine-arfvedsonite granite. Aenigmatite forms fine elongated and bent grains in association with other mafic minerals; astrophyllite crystallizes as tiny needles forming segregations between and inside quartz and albite grains (Fig. 2a). Titanite is a common accessory

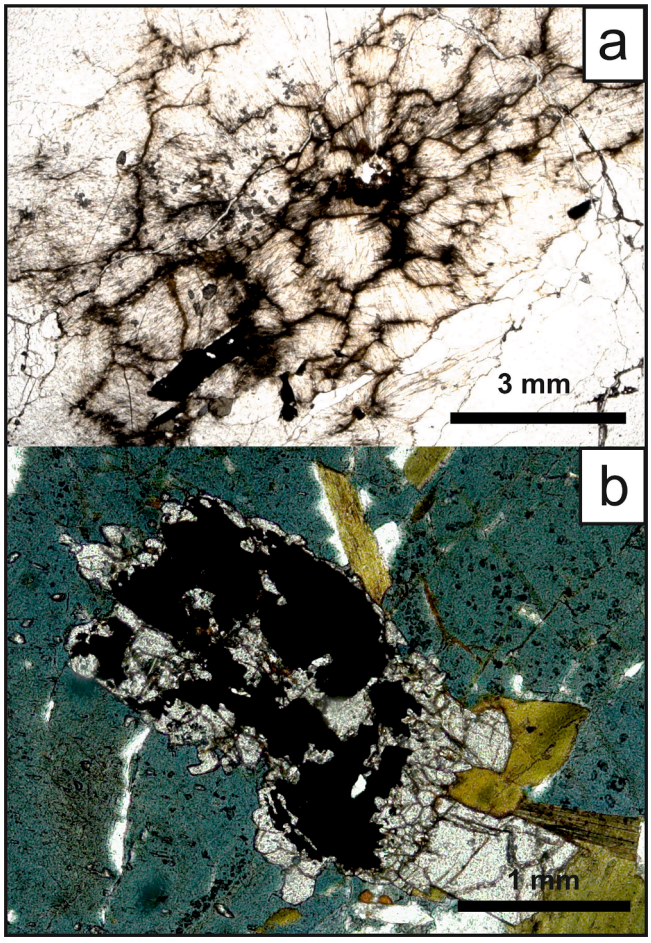

Fig. 2. (a) Astrophyllite needles growing between and inside quartz and K-Na feldspar grains in aegirine-arfvedsonite granite; (b) titanite overgrowing ilmenite in biotite-arfvedsonite granite.

mineral in biotite-bearing granite, forming individual euhedral crystals and overgrowths on ilmenite (Fig. 2b). Quartz veins (a few tens of cm thick and up to ten metres long) containing rare ilmenite plates occasionally cut the granite and are the latest igneous phase.

4.2. Pegmatite bodies

The most abundant rare-element minerals are zircon, fergusonite-(Y), gadolinite-(Y), and thorite. Keivy pegmatites are of the NYF family and gadolinite type, with a Y, HREE, Zr, Ti, Nb (Nb ≫ Ta), F signature according to the classification of Černý and Ercit (2005). In addition to common rare-metal mineralization (zircon, fergusonite-(Y), thorite, monazite-(Ce), allanite-(Ce), kainosite-(Y), astrophyllite, titanite, chevkinite-(Ce), gadolinite-(Y), hingganite-(Y), britholite-group minerals), the White Tundra pegmatite is characterized by abundant galena and secondary REE mineralization (tengerite-(Y), bastnäsite-(Y)). From a compilation of several previous studies (Voloshin et al., 2005; Lyalina et al., 2012, 2014; Zozulya et al., 2020) the inferred crystallization sequence of the main REE and HFSE minerals and titanosilicates in the pegmatite is: zircon – fergusonite-(Y) – monazite-(Ce) – britholite-(Y) – astrophyllite – titanite – allanite-(Ce) — chevkinite-(Ce) – ilmenite – kainosite-(Y) – REE carbonates. Zircon is polygenetic and also forms individual crystals and rims on the late stages of pegmatite formation and the high- to low-temperature hydrothermal stages (Lyalina et al., 2012). All samples contain zircon, kainosite and quartz as the main rock-forming minerals, while astrophyllite, titanite and allanite are less abundant (Figs. 3 and 4). All are included in 1–2 cm anhedral kainosite

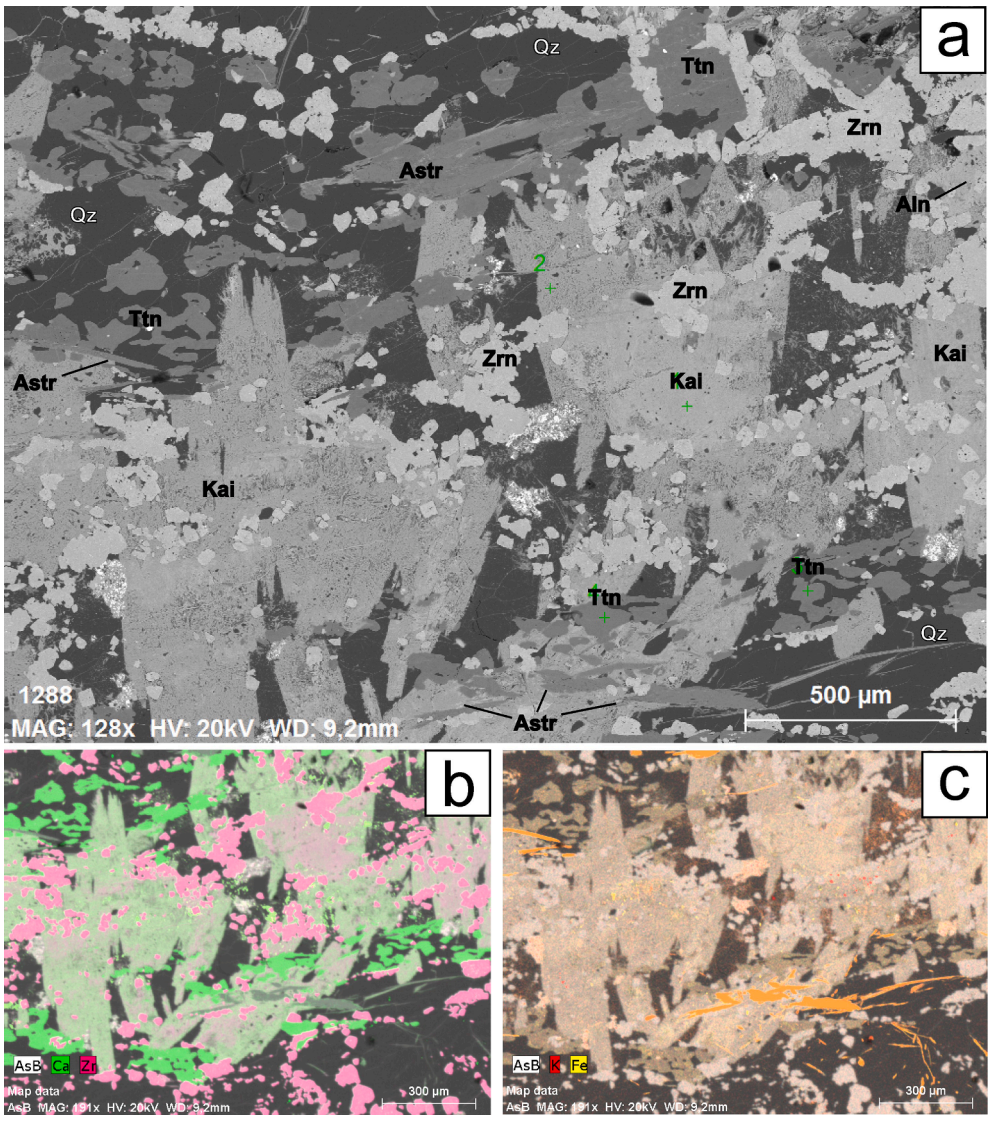

Fig. 3. (a) BSE image showing the typical textural relationships between minerals in samples of White Tundra pegmatite. Astr, astrophyllite; Kai, kainosite; Zrn, zircon; Qz, quartz; Aln, allanite. (b) Element maps for Ca and Zr. (c) Element maps for K and Fe. Maps are for a portion of image (a).

grains. Relationships between allanite and the Ti minerals were not observed, but allanite grew after fergusonite (Zozulya et al., 2020) and after zircon but before kainosite (Fig. 4d).

Astrophyllite in the pegmatite is associated with zircon, titanite and kainosite in a quartz matrix (Figs. 3, 4c). It forms needles and elongated plates up to 700 µm. Plates are often split into elongated fibres and may be cut by thin (1–2 µm) cracks filled with REE carbonate. The grains of astrophyllite have no mineral inclusions or textural zoning. Titanite has been studied from the same mineral association as astrophyllite, where it occurs as anhedral platy grains (up to 300 µm long) with extremely uneven boundaries (Fig. 4a, b). Often it is enclosed in quartz and contains quartz inclusions. A remarkable feature of the titanite is the patchy zoning with low-, medium- and high-intensity in BSE zones of irregular form. No spatial distribution of the different zones in rims or cores is observed. As magmatic and high-T titanites usually show oscillatory or sector zoning, the White Tundra titanite apparently grew at low-T and in a changing chemical environment (e.g., Xiao et al., 2020). Allanite forms isomorphic anhedral grains up to 200 µm (Fig. 4d) and contains numerous quartz inclusions.

5. Whole-rock and mineral chemistry data

5.1. Whole-rocks

Whole-rock chemistry data, including Sm-Nd isotopes, from the White Tundra granites are given in Supplementary Table S2 and show the differences between the different lithologies. Aegirine-bearing granite is peralkaline (mol. (Na + K) > Al) while the biotite-bearing granite is metaluminous (mol. (Na + K) < Al < (Na + K + Ca)) to peraluminous (mol. Al. > (Na + K + Ca)) (Fig. 5). The peralkaline granite has higher values of HFSE and REE than the metaluminous type. Zirconium abundances vary from 500 to 1800 ppm (average 1280 ppm) in peralkaline granite and from 500 to 850 ppm (average 670 ppm) in met- and per-aluminous granite. The same concerns the REE + Y (averages 510 and 380 ppm for peralkaline and met- and per-aluminous granites, respectively), and Nb (averages 58 and 40 ppm, respectively). The enrichments have been explained by derivation of the primary magmas in enriched mantle sources and protracted fractional crystallization (Zozulya et al., 2012).

Two White Tundra granite samples were analyzed for Nd isotopes to check the possible contamination of granite by crustal material. The samples show contrasting values: one is moderately non-radiogenic with

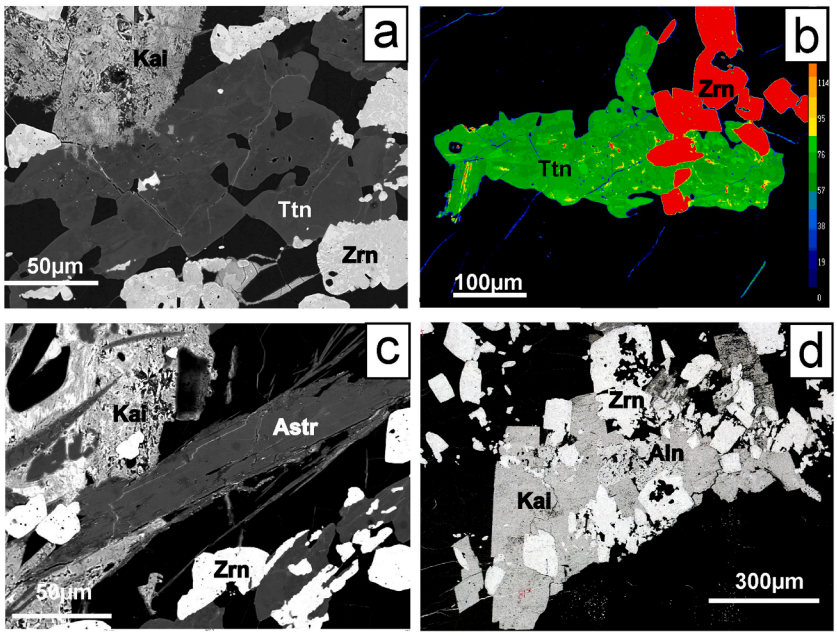

Fig. 4. Association, morphology and internal texture of titanite (a, b) astrophylite (c) and ferriallanite-(Ce) (d) from White Tundra pegmatite. False colour BSE image of titanite (b): the range from dark-green (analyses 12, 38 in Table 2) through green (analyses 8, 10) to light-green (analyses 1, 2, 7, 11, 14) corresponds to an increase of REE + Y; red colour corresponds to zircon.

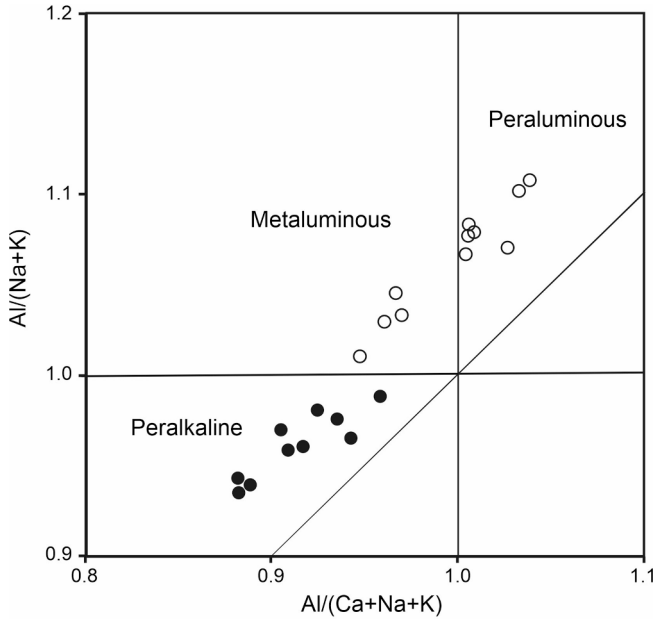

Fig. 5. Alumina saturation index (ASI) diagram for White Tundra granites, showing the continuous trend from peralkaline through metaluminous to peraluminous compositions (solid circles are for aegirine-bearing granite, open circles biotite-bearing granite). The data are from Supplementary Table S2.

of εNd(2655) = −2.1 which corresponds to an enriched mantle source while the second sample has extremely non-radiogenic εNd(2655) = −9 characteristic of rocks of the Archean TTG complex in the Fenno-scandian shield (Daly et al., 1993; Huhma et al., 2012).

5.2. Astrophyllite

The astrophyllite group has the general formula $A_2BC_7D_2T_8O_{26}(OH)_4X_{0-1}$, where A = Na, K, Rb, Cs, H_2O+, H_2O or □; B = Na or Ca; C = Mn, Fe^{2+}, Fe^{3+}, Na, Mg or Zn; D = Ti, Nb, Zr; T = Si, Al; X = F, OH, O or □ (Piilonen et al., 2003). Here, Sr, Rb and Cs have been placed in the A site, Cr and V in C, and Hf, Ta and Sn in D. Analyses of astrophyllite are presented in Table 1 and Supplementary Table S3. Analytical totals are between 95.3 and 97.6 wt%; they are low, partly because all Fe is presented as Fe^{2+} while some is undoubtedly present as Fe^{3+}. Also, water was not determined; it is normally present in astrophyllite in amounts between 2 and 3 wt% (Piilonen et al., 2003) and estimation of water contents in our analyses on the basis of 31 anions pfu gave values of 2.3 to 2.5 wt%. Formulae were calculated on the basis of 20 cations. Average contents of the structural sites are A, 2.14; B, 1.00 (fixed); C, 6.99; D, 2.01, T 7.86, which are reasonably close to stoichiometric, and there is only limited variation in the data set.

As the analyses show almost no variation in Ti/(Ti + Nb) (0.977–0.987, average 0.99), Fe/(Fe + Mn) (0.949–0.960, average 0.96) and Ti/(Ti + Zr) (0.986–0.994, average 0.99) the mineral is near end-member astrophyllite with only minor amounts of the niobophyllite, kupletskite and zircophyllite components. Notable features of the data are the low Na_2O contents; generally in astrophyllite they exceed 2 wt% (Piilonen et al., 2003). We are unaware of any other member of the group where Ta ≈ Nb (average Nb/Ta = 1.0); also the SnO_2 values (0.94–1.19 wt%) and V_2O_3 (0.29–0.35 wt%) are the highest yet recorded, so far as we know.

5.3. Titanite

Compositionally (Table 2 and Supplementary Table S3), the light patches in the titanite have high REE + Y contents (0.050 – 0.061 apfu), the medium patches have lower REE + Y (0.001 – 0.008 apfu) and high Fe (0.129 – 0.143 apfu), and the dark zones correspond to pristine titanite with low REE + Y (0.008 – 0.020 apfu) and Fe (0.025 – 0.041 apfu). Niobium, another important component, ranges from 0.001 to 0.002 apfu in dark patches through 0.004–0.006 apfu in light patches to 0.011–0.034 apfu in medium patches. Overall, compositional variation in the titanite can be expressed by the relationships Al + Fe + Nb + Ta = 2Ti (Fig. 6a) and REE + Y + Na = 2Ca (Fig. 6b), which is in accordance with the main substitutions in titanite (Chakhmouradian, 2004; Vuorinen and Hålenius, 2005; Liferovich and Mitchell, 2006a,b; Kropáč et al., 2020; and references therein). Due to the generally high Fe and low Al

Table 1
Representative compositions of astrophyllite from White Tundra pegmatite.

Sample N° wt. %	1	2	3	4	5	6
SiO_2	32.53	32.53	32.51	32.34	32.11	31.80
Al_2O_3	1.68	1.84	1.76	1.78	1.77	1.69
TiO_2	10.66	10.68	10.74	10.45	10.55	10.75
FeO	34.95	34.15	35.06	34.92	34.71	34.69
MnO	1.48	1.58	1.48	1.52	1.47	1.52
MgO	bd	bd	bd	bd	bd	bd
SnO_2	1.18	1.06	1.11	1.14	1.13	1.07
CaO	2.33	2.36	2.43	2.40	2.51	2.40
Na_2O	1.68	1.61	1.54	1.48	1.31	1.39
K_2O	5.74	6.07	5.97	6.04	6.05	6.37
Nb_2O_5	0.29	0.27	0.26	0.40	0.29	0.30
Ta_2O_5	0.43	0.43	0.34	0.41	0.38	0.52
ZrO_2	0.15	0.17	0.12	0.21	0.21	0.21
HfO_2	0.00	0.00	0.00	0.00	0.00	0.00
V_2O_3	0.33	0.29	0.35	0.34	0.31	0.33
ZnO	0.11	0.09	0.15	0.10	0.12	0.11
SrO	0.00	0.14	0.13	0.13	0.13	0.13
Rb_2O	0.73	0.64	0.62	0.72	0.83	0.50
Cs_2O	0.10	0.13	0.13	0.13	0.14	0.13
F	0.44	0.44	0.38	0.42	0.37	0.38
Cl	bd	0.00	bd	bd	bd	0.00
H_2O	2.43	2.43	2.48	2.44	2.45	2.44
Total	97.23	96.93	97.55	97.37	96.82	96.71
Formulae on the basis of 20 cations (apfu)						
Na*	0.310	0.288	0.267	0.238	0.199	0.207
K	1.667	1.766	1.727	1.753	1.769	1.864
Sr	0.000	0.018	0.017	0.017	0.018	0.017
Rb	0.107	0.093	0.090	0.106	0.122	0.073
Cs	0.010	0.013	0.013	0.013	0.013	0.013
Sum A	*2.09*	*2.18*	*2.11*	*2.13*	*2.12*	*2.17*
Na	0.433	0.422	0.410	0.415	0.384	0.410
Ca	0.567	0.578	0.590	0.585	0.616	0.590
Sum B	*1.00*	*1.00*	*1.00*	*1.00*	*1.00*	*1.00*
Fe^{2+}	6.658	6.512	6.652	6.649	6.658	6.651
Mn	0.285	0.306	0.284	0.294	0.285	0.294
Mg	0.000	0.000	0.000	0.000	0.000	0.000
Zn	0.018	0.015	0.025	0.017	0.020	0.018
V	0.061	0.053	0.064	0.062	0.058	0.061
Sum C	*7.02*	*6.89*	*7.02*	*7.02*	*7.02*	*7.02*
Ti	1.827	1.832	1.832	1.790	1.820	1.853
Nb	0.029	0.028	0.026	0.042	0.030	0.031
Ta	0.027	0.026	0.021	0.025	0.024	0.032
Zr	0.016	0.019	0.013	0.024	0.024	0.024
Hf	0.000	0.000	0.000	0.000	0.000	0.000
Sn	0.120	0.108	0.112	0.116	0.115	0.109
Sum D	*2.02*	*2.01*	*2.01*	*2.00*	*2.01*	*2.05*
Si	7.409	7.416	7.375	7.363	7.364	7.289
Al	0.450	0.496	0.471	0.478	0.478	0.455
Sum T	*7.86*	*7.91*	*7.85*	*7.84*	*7.84*	*7.74*
Σ cations	20.00	20.00	20.00	20.00	20.00	20.00

contents the titanites do not fall into the "igneous" or "metamorphic" fields (Fig. 6c) in the plot of Aleinikoff et al. (2002), pointing to a hydrothermal origin. Titanite also has the lowest ZrO_2/HfO_2 ratios ($\ll 1$) yet known (ZrO_2 is below detection level (~0.07 wt%) whereas HfO_2 ranges from 0.21 to 0.30 wt%). Of interest also are the high WO_3 (0.05–0.49, average 0.19 wt%), V_2O_3 (0.96–1.17, average 1.06 wt%) and SnO_2 (0.6–2.1, average 1.03 wt%). Chondrite-normalized REE plots show a highly unfractionated pattern with Ce/Y_n varying from 0.08 to 0.03 (Fig. 7).

5.4. Ti-rich ferriallanite-(Ce)

Allanite, an REE-Th-rich member of the epidote supergroup, has the general formula $(Ca,Ce,La,Nd,Th)_2(Fe^{2+},Fe^{3+},Ti)(Al,Fe^{3+})_2Si_3O_{12}(OH)$. Representative analyses of ferriallanite-(Ce) are given in Table 3; the full data set is in Supplementary Table S3. Formulae have been calculated on the basis of 12.5 oxygens. Analytical totals are in the range 95.97–98.97 wt% (average 97.61 wt%), partly because total Fe is presented as Fe^{2+} whereas there is significant Fe^{3+} (see below) and perhaps partly because the minerals have been secondarily hydrated. The cation sums range from 8.11 to 8.19 apfu (average 8.15 apfu), slightly higher than the theoretical 8 but again at least partly a result of presenting all Fe as Fe^{2+}. The $Fe^{3+}/(Fe^{2+} + Fe^{3+})$ ratios, calculated from stoichiometry, are in the range 0.18–0.31 (Supplementary Table S3). The ferriallanite-(Ce) is remarkable for one of the highest contents of TiO_2 (2.77–4.49 wt%, average 3.59 wt%). Normally, allanite contains 1 to 2 wt% of TiO_2 and only the altered mineral has elevated values up to 4.67 wt% (see review in Gieré and Sorensen (2004)).

Compositions are plotted in the (REE + Y + Sr + Th + Mn) vs Al diagram of Petrik et al. (1995) in Fig. 8a. The analyses cluster close to the ferriallanite-(Ce) composition, with a slight elongation along the $REE^{3+} + Fe^{2+} = Ca^{2+} + Al^{3+}$ line. Nevertheless, the major portion of analyses fall beyond the stoichiometric compositions for allanites with Al ranging from 0.7 to 1.0 apfu. A good negative correlation between Fe + Ti and Al (Fig. 8b) indicates that incorporation of a large amount of Ti into the ferriallanite-(Ce) via the coupled substitution $Ti^{4+} + Fe^{2+} = 2Al^{3+}$ (Vlach and Gualda, 2007; Bagiński et al., 2016) was a reason for the stoichiometry discrepancy.

The ferriallanite-(Ce) is strongly LREE-enriched, with elements heavier than Gd below detection level and a highly fractionated chondrite-normalized pattern (Fig. 7). Yttrium oxide levels are $\leq$ 0.28 wt% and Ce/Y_n varies from 160 to 340. Most samples have modest positive Ce anomalies (Ce/Ce* 1.1–1.4).

6. Nb-Ta, Zr-Hf and REE fractionation in Ti minerals from the White Tundra pegmatite with implications for ore-forming processes

Trace element incorporation into minerals seems to be controlled by three factors; (1) source composition, which controls the availability of particular trace elements (in granitic and/or pegmatitic systems in our case); (2) processes that govern the partitioning of a particular trace element (Nb against Ta, Zr against Hf, partitioning of individual REEs, in our case) with two aspects: (a) fractional crystallization during the magmatic stage, and (b) changing fluid composition during the late- to post-magmatic stages; and (3) crystallochemical factors which may allow incorporating a specific trace element from "geochemical twins" (like Nb-Ta and Zr-Hf). The experimental data indicate that with the same source and processes the third factor seems to be not crucial, as was shown by the crystallochemical studies of Liferovich and Mitchell (2006a,b) for incorporation of Nb and Ta into synthetic titanite. Natural titanite from a number of localities may accept high concentrations of Nb or Ta, or both (Clark, 1974; Paul et al., 1981; Groat et al., 1985; Bernau and Franz, 1987; Černý et al., 1995), confirming the absence of a structurally controlled preference. Therefore we now discuss mainly the first two factors in relation to the White Tundra pegmatite.

6.1. Granite-pegmatite system

As the White Tundra massif is composed of a differentiated rock series and the pegmatite has a multistage (from late-magmatic to hydrothermal) origin, it might be expected that there were variations in the Nb/Ta ratios. Indeed, the ratios in the alkali feldspar granite range from 14 to 21 (average 17). The variation correlates positively with the agpaitic index (Fig. 9), in accord with overall observations of higher Nb/Ta in agpaitic rocks than the same ratio in miaskitic types (Ballouard et al., 2020; Lowery Claiborne et al., 2006; Skosyreva and Solodov, 1983; Kuz'menko, 1978; and references therein). The lower Nb/Ta ratios in the biotite-bearing lithologies were cautiously explained by assimilation of upper crustal rocks, shown by the presence of xenoliths and Nd isotope data (Sections "Geological background" and "Whole-rock and mineral chemistry data"). The pegmatite is located in biotite-bearing granite and it may be inferred that the residual pegmatitic

Table 2
Representative compositions of titanite from White Tundra pegmatite.

Sample N⁰	1	2	7	11	14	8	10	12	38
	Bright patches					Gray patches		Dark-gray patches	
wt. %									
SiO_2	28.29	28.37	28.71	28.34	28.65	29.64	29.36	29.04	28.87
Al_2O_3	0.75	0.74	0.59	0.75	0.70	1.82	1.72	0.17	0.23
TiO_2	34.26	33.94	35.28	34.26	34.59	31.41	30.94	38.83	36.56
Fe_2O_3	3.07	3.06	2.72	3.25	3.04	5.28	5.17	1.02	1.40
MnO	0.14	0.09	0.07	0.08	0.13	bd	bd	bd	bd
SnO_2	1.09	1.22	1.00	1.24	1.07	0.55	0.57	0.65	2.08
CaO	23.77	23.71	24.63	24.07	24.50	28.44	28.12	27.23	26.36
Na_2O	0.87	0.93	0.85	0.88	0.78	0.07	0.07	0.52	0.64
Ce_2O_3	0.08	bd	bd	bd	0.08	bd	bd	bd	bd
Nd_2O_3	bd	0.16	bd	bd	bd	bd	bd	0.25	0.26
Gd_2O_3	0.16	0.15	bd	0.13	0.18	bd	bd	bd	bd
Dy_2O_3	bd	0.55	0.38	0.29	0.36	bd	bd	bd	bd
Ho_2O_3	bd	0.15	bd	bd	bd	bd	bd	bd	bd
Er_2O_3	0.20	0.33	0.27	0.33	0.28	bd	bd	bd	bd
Yb_2O_3	0.30	0.36	0.32	0.37	0.34	bd	bd	bd	bd
Y_2O_3	3.36	3.40	2.80	3.17	3.11	0.20	0.11	0.50	0.44
Nb_2O_5	0.34	0.36	0.33	0.44	0.26	0.75	0.80	bd	0.10
Ta_2O_5	0.58	0.65	0.67	0.74	0.64	0.50	0.45	0.31	1.26
ZrO_2	bd	bd	bd	bd	bd	bd	bd	bd	bd
HfO_2	0.26	0.26	0.27	0.25	0.27	0.25	0.23	0.28	0.27
WO_3	0.16	0.13	0.20	0.21	0.18	0.24	0.24	0.23	0.48
V_2O_3	1.08	1.09	1.08	1.02	1.10	0.96	0.98	1.17	1.16
Total	98.77	99.64	100.17	99.78	100.23	100.09	98.76	100.20	100.09
Formulae on the basis of 3 cations									
Si	0.958	0.959	0.958	0.954	0.958	0.966	0.970	0.952	0.957
Al	0.030	0.029	0.023	0.030	0.028	0.070	0.067	0.007	0.009
Ti	0.872	0.863	0.886	0.867	0.870	0.770	0.769	0.957	0.912
Fe^{3+}	0.078	0.078	0.068	0.082	0.076	0.129	0.129	0.025	0.035
Mn	0.004	0.003	0.002	0.002	0.004	0.001	0.000	0.001	0.001
Sn	0.016	0.018	0.015	0.019	0.016	0.008	0.008	0.010	0.031
Ca	0.862	0.858	0.881	0.868	0.878	0.993	0.996	0.956	0.937
Na	0.057	0.061	0.055	0.057	0.051	0.004	0.005	0.033	0.041
Ce	0.001	0.001	0.001	0.001	0.001	0.000	0.000	0.000	0.000
Nd	0.001	0.002	0.000	0.000	0.001	0.000	0.000	0.003	0.003
Gd	0.002	0.002	0.001	0.001	0.002	0.000	0.000	0.000	0.000
Dy	0.002	0.006	0.004	0.003	0.004	0.000	0.000	0.000	0.000
Ho	0.001	0.002	0.001	0.001	0.001	0.000	0.000	0.000	0.000
Er	0.002	0.003	0.003	0.003	0.003	0.001	0.000	0.000	0.000
Yb	0.003	0.004	0.003	0.004	0.003	0.000	0.000	0.000	0.000
Y	0.061	0.061	0.050	0.057	0.055	0.003	0.002	0.009	0.008
Nb	0.005	0.005	0.005	0.007	0.004	0.011	0.012	0.001	0.002
Ta	0.005	0.006	0.006	0.007	0.006	0.004	0.004	0.003	0.011
Zr	0.000	0.000	0.000	0.000	0.000	0.001	0.001	0.000	0.000
Hf	0.003	0.002	0.003	0.002	0.003	0.002	0.002	0.003	0.003
W	0.004	0.003	0.005	0.005	0.005	0.006	0.006	0.006	0.012
V	0.029	0.030	0.029	0.028	0.029	0.025	0.026	0.031	0.031
Σ cations	3.000	3.000	3.000	3.000	3.000	3.000	3.000	3.000	3.000

melt had Nb/Ta ratios of ≤ 15. Early-crystallized fergusonite with much higher Nb/Ta ratios (70–440, average 190; Zozulya et al., 2020) consumed more Nb than Ta from the pegmatitic melt and may have induced a decrease of Nb/Ta ratio in the residual melt/solution and the possible crystallization of later minerals with unusually low Nb/Ta ratios, such as astrophyllite (average 1.0) and titanite (average 1.2).

To some extent the assimilation of upper crustal lithologies could also have been responsible for increases of Sn, W and V in the pegmatitic system and resulted in elevated values of these elements in astrophyllite, titanite and ferriallanite-(Ce).

The main factors which can fractionate Zr from Hf are fractional crystallization of granitic magma and temperature decrease (Wang et al., 2010); when the crystal structure of the main host mineral (zircon) contracts, increasing the ability of the smaller Hf ion to enter the structure. Experimental studies of Zr and Hf solubility in silicate melts of various composition have demonstrated that Zr and Hf solubilities depend on the alumina-saturation index (ASI) of the melt. With a high molar Al/(Ca + Na + K) ratio the Zr/Hf value decreases in zircon and consequently in the host rock (Linnen and Keppler, 2002; Yin et al., 2013; Aseri et al., 2015). The White Tundra granites show a distinct Zr/Hf decrease in the non-agpaitic facies (Figs. 3, 9). Lyalina et al (2012) demonstrated that the Zr/Hf ratio in magmatic zircon from the Keivy agpaitic granite ranges from 41 to 58 (average 48), almost the same as in the bulk rock. As zircon is a good indicator of Zr/Hf in the host rock, it might be expected the ratio would be lower in minerals from the pegmatite - ≤30, as was predicted earlier. However, the pegmatitic zircon has much lower Zr/Hf (from 14 to 23), decreasing from early stage to late-stage zircon [averages 20 and 15, respectively] (Lyalina et al., 2012; Supplementary Table S4). Thus, the pegmatitic system was enriched in Hf from the beginning of crystallization and became successively more enriched, allowing the appearance of (Zr, Hf)-bearing minerals with anomalously low Zr/Hf ratios during the late stages of pegmatite crystallization.

A change of bulk rock composition may also have happened during evolution of the pegmatite itself. Earlier (Section "Geological Background") it was demonstrated that Zr minerals indicate a transition between agpaitic and miaskitic compositions showing crystallization of zirconosilicates and zircon at different stages. In addition to the report by Voloshin et al. (2005) of quartz-zircon pseudomorphs on zirconosilicate, we have documented here a hypothetical "Ca-REE-

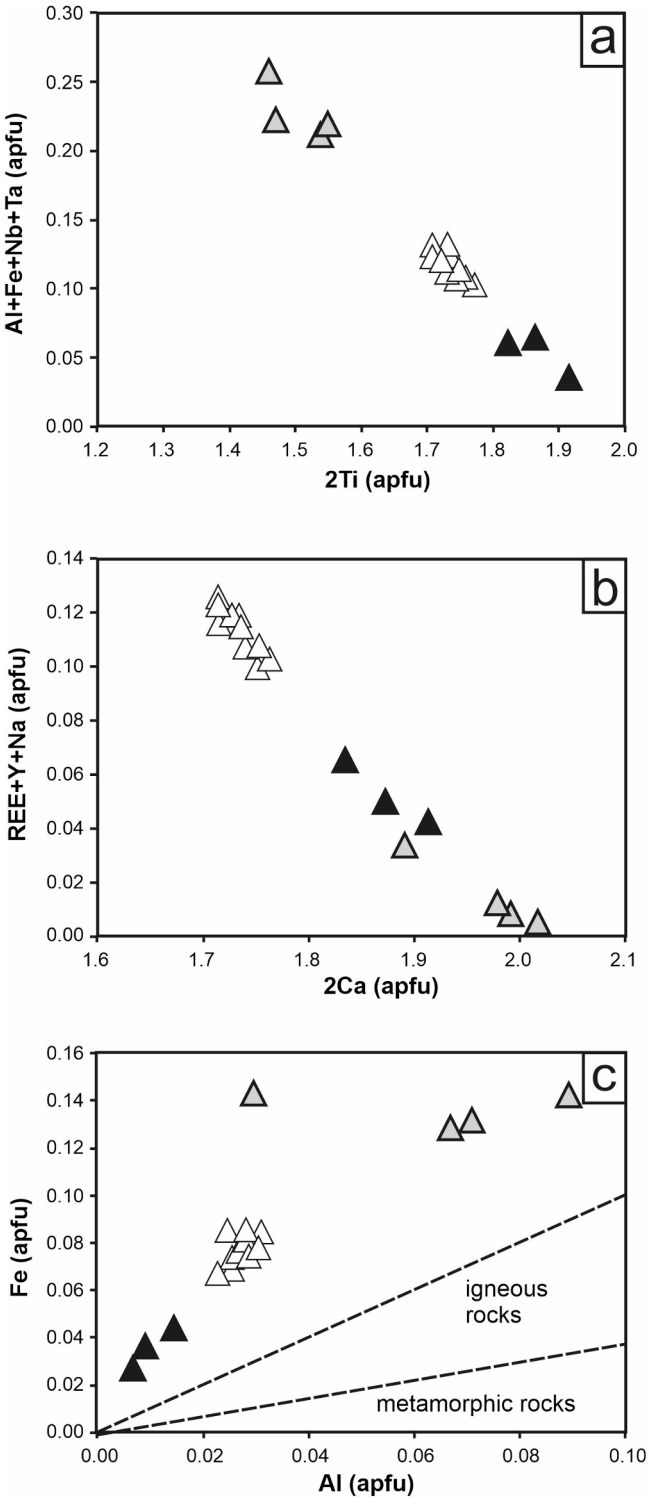

Fig. 6. Titanite compositional variation. (a) Al + Fe + Nb + Ta vs. 2Ti and (b) REE + Y + Na vs. 2Ca; (c) Al vs. Fe diagram according to Aleinikoff et al. (2002) depicting the possible origin of titanite. Solid triangles are for dark-gray patches, gray triangles – for gray patches, open triangles – for light patches.

zirconosilicate" included in zircon (analysis 6/1, Supplementary Table S4). Astrophyllite and titanite are also members of agpaitic and miaskitic assemblages, respectively. Thus the pegmatite exhibits the transition between these assemblages with decreases in Nb/Ta and Zr/Hf in its bulk composition. The agpaitic to miaskitic transition in pegmatite is thought to have been a result of contamination by upper

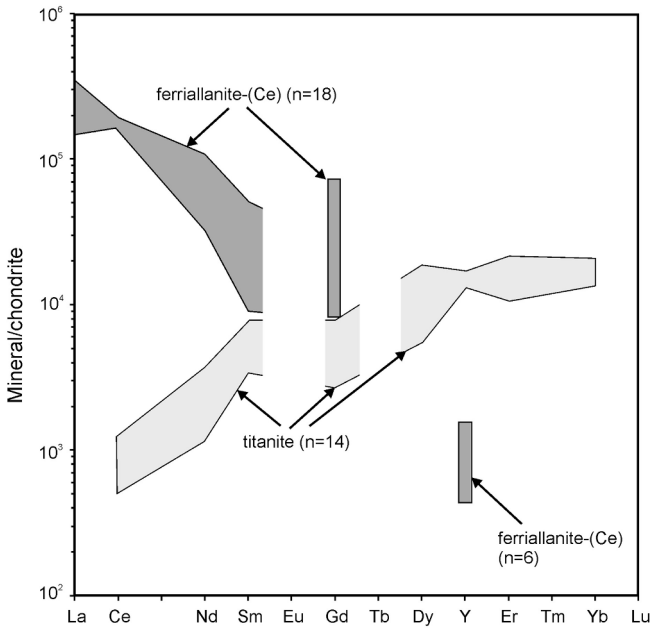

Fig. 7. Chondrite-normalized REE patterns for titanite and ferriallanite from White Tundra pegmatite. Normalizing factors from Sun and McDonough (1989).

Table 3
Representative compositions of ferriallanite-(Ce) from White Tundra pegmatite.

Sample №	1	2	6	15	16	21
wt. %						
SiO_2	29.84	29.91	29.46	29.28	29.52	29.38
Al_2O_3	6.87	7.64	6.78	7.97	7.98	6.95
TiO_2	4.04	3.56	4.24	3.17	3.34	3.30
FeO_{tot}	21.84	21.24	21.65	21.14	20.76	22.03
MnO	0.24	0.26	0.31	0.20	0.24	0.37
MgO	bd	bd	bd	bd	bd	bd
CaO	8.79	9.18	8.70	9.12	8.99	8.78
Na_2O	bd	0.19	0.28	0.14	0.13	0.18
La_2O_3	4.85	4.44	5.72	4.26	4.83	8.06
Ce_2O_3	13.14	12.68	13.63	12.71	13.19	13.55
Pr_2O_3	1.36	1.58	1.31	1.36	1.23	0.98
Nd_2O_3	5.40	5.36	3.96	5.71	4.82	2.26
Sm_2O_3	0.74	0.84	0.16	0.86	0.74	bd
Gd_2O_3	1.43	1.43	1.34	1.57	1.49	1.36
Y_2O_3	0.23	bd	0.28	bd	bd	bd
ThO_2	0.12	bd	bd	bd	bd	0.16
Total	98.97	98.41	97.82	97.52	97.26	97.38
Formulae on the basis of 12.5 oxygens						
Ca	0.977	1.018	0.976	1.023	1.007	0.993
Na	0.005	0.012	0.018	0.009	0.008	0.011
La	0.186	0.169	0.221	0.164	0.186	0.314
Ce	0.499	0.480	0.522	0.487	0.505	0.524
Pr	0.017	0.019	0.016	0.016	0.015	0.012
Nd	0.200	0.198	0.148	0.213	0.180	0.085
Sm	0.026	0.030	0.006	0.031	0.027	0.000
Gd	0.049	0.049	0.046	0.054	0.052	0.048
Y	0.013	0.000	0.016	0.000	0.000	0.000
Th	0.003	0.002	0.000	0.000	0.000	0.004
Sum A	*1.97*	*1.98*	*1.97*	*2.00*	*1.98*	*1.99*
Al	0.840	0.932	0.836	0.983	0.983	0.865
Ti	0.315	0.277	0.334	0.250	0.263	0.262
Fe^{2+}	1.894	1.838	1.895	1.850	1.815	1.944
Mn	0.007	0.007	0.009	0.006	0.007	0.010
Mg	0.000	0.000	0.000	0.000	0.000	0.000
Sum M	*3.06*	*3.05*	*3.07*	*3.09*	*3.07*	*3.08*
Si	3.095	3.095	3.083	3.065	3.086	3.101
Σ cations	8.12	8.13	8.12	8.16	8.13	8.17

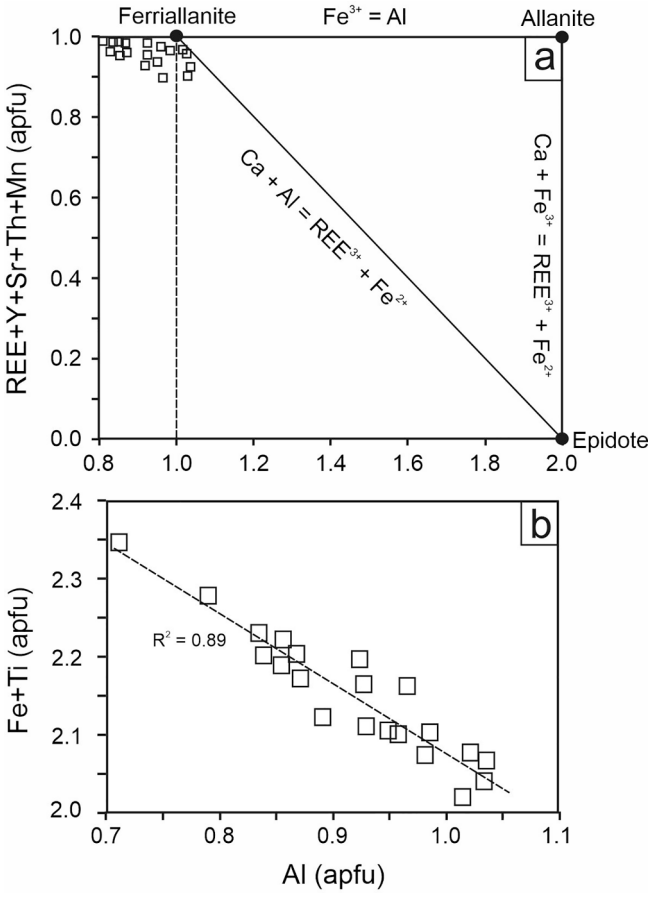

Fig. 8. (a) Ferriallanite-(Ce) on the (REE + Y + Sr + Th + Mn) vs Al classification diagram of Petrik et al. (1995). (b) negative correlation of Fe + Ti and Al.

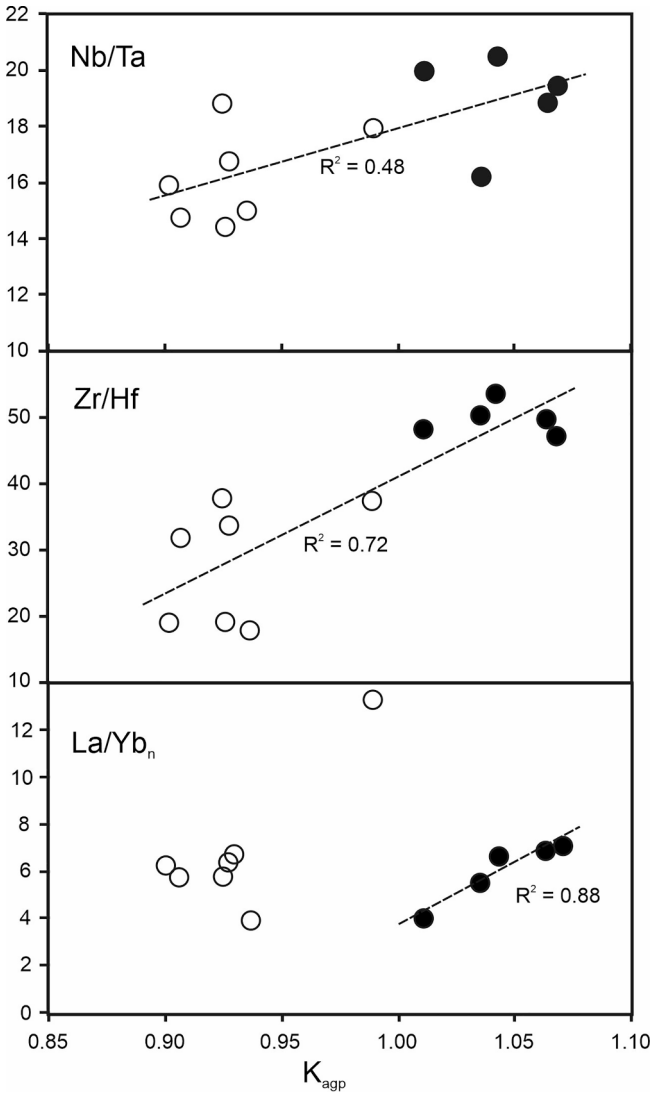

Fig. 9. Nb/Ta, Zr/Hf, La/Yb_n vs K_{agp} plots for White Tundra granites. Symbols as for Fig. 5. The data are from Supplementary Table S2.

crust material with enhanced Ta and Hf contents. High agpaicity conditions for the early-stage pegmatite can be suggested from the positive correlation of K_{agp} and La/Yb_n in peralkaline granite facies (Fig. 9), showing the higher rate of REE fractionation with K_{agp} increase.

Astrophyllite and titanite from the pegmatite show a clear fractionation of the Zr-Hf pair. The first mineral has Zr/Hf ≫ 1, whereas the second has Zr/Hf < 1. Despite the zircon from the pegmatite having lower Zr/Hf than the parental granite (but still > 1) and reflecting the bulk pegmatite composition, its crystallization at numerous stages cannot alone have caused the change of Zr/Hf from astrophylite to titanite. Perhaps hydrothermal processes were also responsible for the Zr/Hf ratios being < 1 in titanite.

6.2. Role of hydrothermal processes

Undoubtedly, fractional crystallization and contamination in the White Tundra granite played significant roles in the origin of the pegmatitic melt with decreased Nb/Ta and Zr/Hf ratios and extremely high REE contents. But the anomalous compositions of Ti minerals in White Tundra pegmatites with Nb < Ta and Zr < Hf, and high Y + HREE cannot be explained without the involvement of hydrothermal processes. There is in the literature mineralogical evidence for Ta and Hf hydrothermal enrichment in Nb-Ta-oxides and Zr-Hf-silicates, respectively. Overgrowths of hydrothermal tantalite on magmatic columbite have been observed in rare-metal granites and related Nb-Ta-Sn deposits in south China (Zhu et al., 2015; Xie et al., 2016). Ta-rich fergusonite and formanite overgrowths on early Nb-rich fergusonite are documented in pegmatites related to the Keivy alkali feldspar granite (see review in Zozulya et al (2020)). Few experimental studies of Nb and Ta solubility in aqueous solution exist, but Ta seems to be less soluble than Nb (e.g., Zaraisky et al., 2010). Therefore, it is suggested that during hydrothermal alteration, Ta will preferentially form overgrowths around Nb-Ta–bearing minerals, whereas Nb will be carried away by fluids. Again, the role of F is significant, as with high F activity in a hydrothermal solution Nb solubility increases considerably, while Ta becomes more mobile than Nb (Černý and Ercit, 1989; Tiepolo et al., 2002; Smith et al., 2009; Ballouard et al., 2016, 2020). For example, a crucial role of fluorine in the remarkable Ta > Nb composition of titanite from the Maršikov pegmatite has been suggested (Černý and Ercit, 1989; Černý et al., 1995).

Trace Nb and Ta mainly substitute for Ti (with charge balancing by Fe) in titanosilicates. Thus, a possible link between Nb/Ta, Ti and Fe would be expected in Ti minerals from the White Tundra pegmatite. Titanite clearly shows a change of Nb/Ta ratio during crystallization at different stages, ranging from 0.1 to 1.6 (Fig. 10a). It is noteworthy that the lowest Nb/Ta ratios (0.1–0.2) are found in pristine titanite with formulae-normal TiO_2 concentrations, 0.3.-0.7 in Y-HREE rich titanite with lower TiO_2 (34–35 wt%) and elevated Fe_2O_3 (2.9–3.3 wt%), and the highest Nb/Ta (1.2–1.6) in titanite with non-stoichiometric TiO_2 (28–31 wt%) and high Fe_2O_3 (5.2–5.7 wt%). Nb/Ta positively correlates with Nb (Fig. 10b), which contradicts the overall behavior of Nb and Ta in natural samples (usually the Nb/Ta ratio tends to anticorrelate with Nb and Ta contents (Ballouard et al., 2020)) and suggests disequilibrium

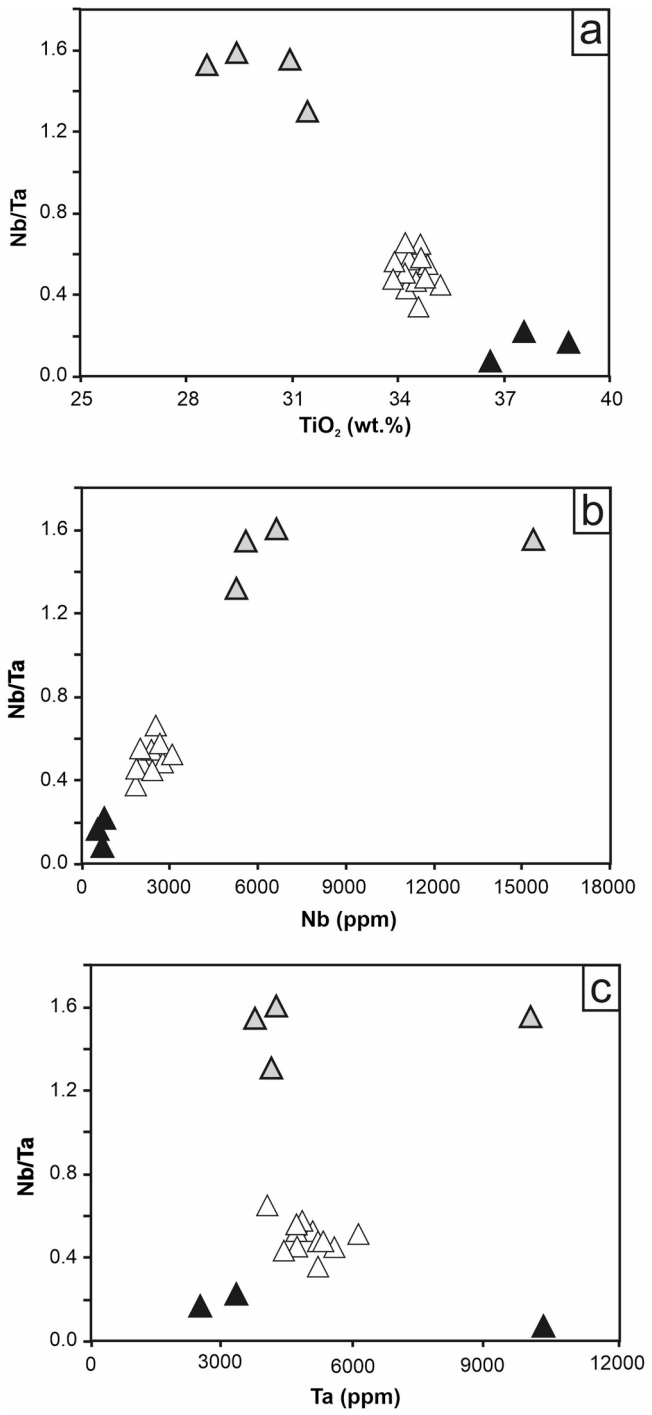

Fig. 10. Nb/Ta vs TiO_2, Nb, Ta in titanite from White Tundra pegmatite, showing the different behaviour of elements and ratios. Symbols as for Fig. 6.

crystallization of titanite. Coupled with the absence of a correlation between Nb/Ta and Ta (Fig. 10c) this correlation suggests that a Nb decrease at different stages of titanite crystallization is responsible for the lowering of Nb/Ta.

Astrophyllite, in turn, has no correlation between Nb/Ta and TiO_2 (Fig. 11a), pointing to its crystallization during a single stage, and according to Nb/Ta values (0.3–0.8) possibly correlated to the stage of Y-HREE-rich titanite. The Nb/Ta ratio in astrophyllite shows no correlation with Nb and negatively correlates with Ta (Fig. 11b, c), thus Ta increase influenced the Nb/Ta decrease. Apparently, the different activities of Nb and Ta during pegmatite crystallization observed in

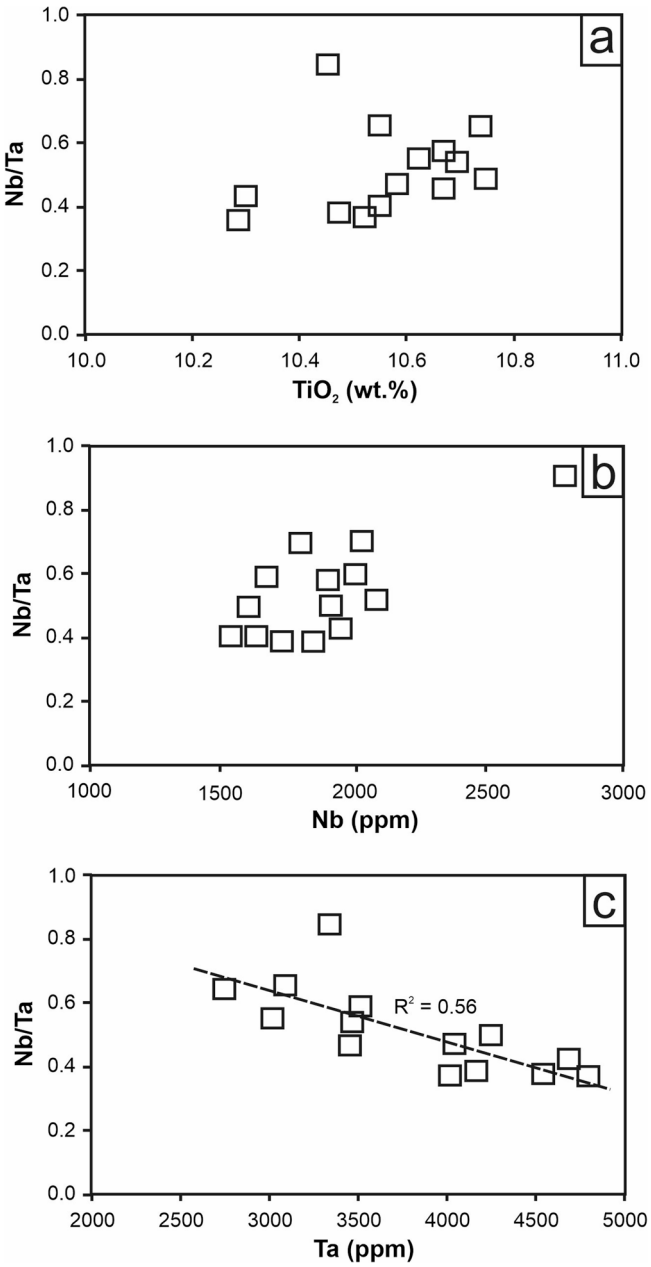

Fig. 11. Nb/Ta vs TiO_2, Nb, Ta in astrophyllite from White Tundra pegmatite, showing the different behaviour of elements and ratios.

titanite depended on a change of F content in the fluid/solution, as was discussed above and confirmed by studies of fluorbritholite-(Y) and fergusonite-(Y) from the pegmatite (Zozulya et al., 2019, 2020).

Hf enrichment under hydrothermal conditions is well documented in zircons from LCT-family pegmatites (e.g., Neves et al., 1974; Jacobsen et al., 2007; Yin et al., 2013; Kudryashov et al., 2020). This fractionation of Hf from Zr at the late hydrothermal stages has been linked to the lower mobility of Hf (Gerasimovskiy et al., 1972; Smith et al., 1987; Wang et al., 2010) and supported by experimental data on variable Zr and Hf solubilities in ASI-high melts/fluids under the changing activity of a number of fluxes and volatiles, including fluorine (Keppler, 1993; Aseri et al., 2015; and references therein). Thus, the observed Zr/Hf ratios (<1) in titanite from the White Tundra pegmatite can be interpreted as crystallization in a low-temperature, aluminium-saturated environment with a high F content.

The variability of fluorine and other major fluid components in pegmatitic/hydrothermal environments has been studied using REE-

bearing minerals. It has been theoretically substantiated that Y/Dy and Y/Er ratios in minerals are pointers to F activity (Gramaccioli et al., 1999); this was applied to REE-bearing minerals from the White Tundra pegmatite by Zozulya et al. (2019, 2020). La/Ndn from REE minerals is an effective indicator of CO_2/H_2O change in hydrothermal fluids (Smith et al., 2000), and Ce/Ce* can provide information on oxygen fugacity.

Y and Er fluoride complexes are more stable than Dy fluoride complexes; the stability constants for YF^{2+} and ErF^{2+} are nearly three times as high as the corresponding complex of Dy. Fluorine enrichment during crystallization will result in successive increases of the Y/Dy and Er/Dy ratios in the fluid until crystallization of F-rich minerals (normally fluorite, in some cases fluorapatite, fluorbritholite, fluorthalenite) occurs. The consumption of F destabilizes the Y-F and Er-F complexes, resulting in the local crystallization of REE minerals with higher Y/Dy and Er/Dy ratios. At that stage, Dy will tend to enter any REE minerals formed more efficiently than Y.

Fractionation of La from Nd depends on the CO_2 content in the mineral-forming solutions, affecting the $[La/Nd]_n$ ratio in REE minerals (>4 for CO_2-rich solution,<4 for H_2O-rich solution). Since the paragenetic environment studied in Smith et al. (2000) differs from those of the White Tundra occurrence, the conclusions given below are indirect.

The following model has been constructed from available data on titanite, ferriallanite-(Ce) and kainosite-(Y), and with the involvement of published material from fergusonite-(Y) and fluorbritholite-(Y) from the White Tundra pegmatite (Zozulya et al., 2019, 2020) with the presumed sequence of crystallization fergusonite (1) → fluorbritholite →/= fergusonite (2) → titanite →/= allanite → kainosite. The lowest Y/Dy (2–4) and Y/Er (3–5) ratios are in the earliest fergusonite (1), indicating a high F content of the fluid just emanating from the parent granite. The second stage fluorbritholite and fergusonite (2) with higher Y/Dy (8–12) and Y/Er (5–9) point to a lowering of F, possibly due to its consumption by F-bearing minerals. Nevertheless, during the following stages the F content in the fluid rose again as titanite and kainosite show elevated Y/Dy and Er/Dy ratios (up to 6 and 7, respectively (Fig. 12)). The $[La/Nd]_n$ ratio is below 4 for all minerals (except for single points in ferriallanite) from all stages (Fig. 12; and data in Zozulya et al. (2019, 2020), pointing to a relatively high H_2O/CO_2 ratio in the fluids during the crystallization of the pegmatite. Positive Ce/Ce* anomalies for most minerals from all stages indicate overall oxidized conditions during crystallization of the pegmatite, except for late stage kainosite-(Y) with Ce/Ce* ranging from 0.1 to 1 (Fig. 12).

The proposed model is in accord with the balance of Nb and Ta in the pegmatite: the early crystallized fergusonite consumed more Nb, causing a decrease of Nb/Ta in the system; the changing F content and temperature drop during late stages could have enhanced the Nb/Ta decrease to anomalous values (<1), as is observed in titanite and astrophyllite.

6.3. *Implications for ore-forming processes*

The fractionation processes studied here, especially those leading to enrichment of Ta and HREE in pegmatitic-hydrothermal systems, have an economic importance. These “strategic” metals can occur simultaneously due to the conjunction of several processes which happen, for example, in the mixed NYF (Nb-Y-F) – LCT (Li-Cs-Ta) family of pegmatites (according to classification of Černý and Ercit (2005). Contamination of NYF magma with enriched upper crustal lithologies, anatexis of mixed depleted and enriched protholiths and partial depletion of crustal protholiths have been suggested for their genesis (Černý and Ercit, 2005). One of the Keivy rare-metal deposits is the unique Ploskaya Mt pegmatite of amazonite-quartz-albite composition. It is several hundred meters long and several tens of meters wide. Rare-metal mineralization is represented by diverse and abundant REE, Y, Nb, Ta and Li minerals and has a Y, Yb, Nb, Ta, F, P, Li, Be, Sn (Pb, W, Mo) geochemical signature. The high contents of fluorite, yttrofluorite and REE-carbonates point to an important role for volatiles at the

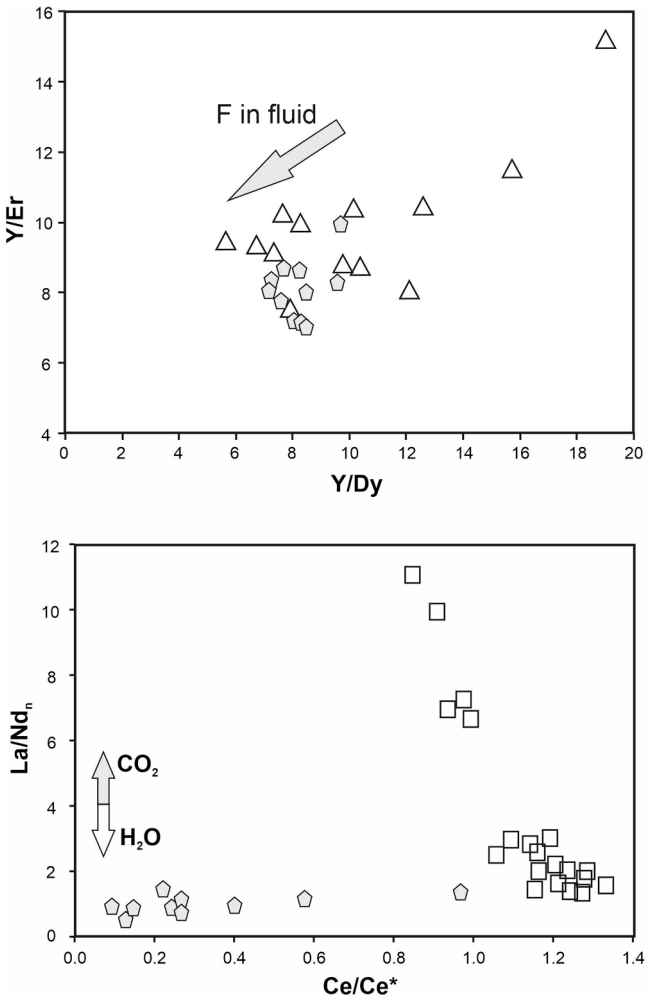

Fig. 12. Y/Dy vs Y/Er and Ce/Ce* vs La/Nd_n plots showing the change of fluid composition during crystallization of titanite, ferriallanite-(Ce) and associated kainosite-(Y) according to models of Gramaccioli et al. (1999) and Smith et al. (2000). Same symbols as in Figs. 6 and 8. Gray pentagon is for kainosite (data are from Supplementary Table S4).

hydrothermal stages of pegmatite formation. At these stages the Ta-rich niobium oxides (e.g. fergusonite-(Y)) and latest tantalum oxides (e.g. formanite-(Y)) crystallize in association with selective HREE minerals (keyviite-(Yb), xenotime-(Yb), hingganite-(Yb)) (Voloshin and Pakhomovskii, 1986).

In the White Tundra case, the pegmatite crystallized from a NYF source contaminated by upper crustal lithologies and is thus considered as a possible precursor of a mixed NYF-LCT family (increase of Ta/Nb ratios in the system but with an absence of the Li-Cs-Be minerals, characteristic of LCT). Ta instead of Nb is incorporated into NYF-type Ti minerals, such as astrophyllite and titanite in the White Tundra pegmatite. The low-temperature hydrothermal environment of the late stage with high and alternating activities of F and CO_2 promoted crystallization of Y-rich minerals, including titanite and REE-carbonates. Both factors can be regarded as crucial in the formation of complex Nb-Ta-Y-HREE pegmatitic deposits associated with rare-metal granitoid magmatism.

7. Conclusions

Fractionation of Nb-Ta, Zr-Hf and REE in the White Tundra pegmatite and crystallization of Ti minerals with anomalous compositions, including low (even < 1) Nb/Ta and Zr/Hf ratios in astrophyllite and

titanite; extremely high contents of Y + HREE in titanite and Ti in ferriallanite, were due to a combination of several factors: (1) the primary source (alkali feldspar granite magma) was very rich in Y + REE, Zr, Nb, Ti; (2) assimilation by primary magma of upper crustal lithologies enriched in Ta, Hf and LREE; (3) transition of HFSE mineral assemblages in the pegmatite from agpaitic to miaskitic with consequent lowering of Nb/Ta and Zr/Hf; (4) crystallization of minerals in a low-temperature (hydrothermal) environment with changing F and CO_2 activities, that promoted a sporadic further decrease of Nb/Ta and Zr/Hf (to values < 1) and an increase of Y + HREE contents. These factors are almost certainly applicable to the genesis of mixed NYF-LCT fertile granite-pegmatite systems with valuable Ta-Y-HREE mineralization.

Declaration of Competing Interest

The authors declare that they have no known competing financial interests or personal relationships that could have appeared to influence the work reported in this paper.

Acknowledgments

We are grateful to Beata Marciniak-Maliszewska from the Inter-Institute Analytical Complex at the Department of Geochemistry, Mineralogy, and Petrology, University of Warsaw, for technical assistance with microprobe analyses. Two anonymous referees and Associate Editor Dr. Alexander Yakubchuk are thanked for very helpful journal reviews and constructive comments. This research was funded by Russian Government grant AAAA-A19-119100290147-7 and by the National Science Centre Poland grant number 2017/26/M/ST10/00407.

Appendix A. Supplementary data

Supplementary data to this article can be found online at https://doi.org/10.1016/j.oregeorev.2022.104779.

References

Aleinikoff, J.N., Wintsch, R.P., Fanning, M.C., Dorais, M.J., 2002. U-Pb geochronology of zircon and polygenetic titanite from the Glastonbury Complex, Connecticut, USA: an integrated SEM, EMPA, TIMS, and SHRIMP study. Chem. Geol. 188, 125–147.

Alekseev, V.I., Marin, Y.B., Gembitskaya, I.M., 2013. Allanite-(Y) in areas of ongonite magmatism in the Far East: isomorphism and petrogenetic implications. Geol. Ore Depos. 55, 503–514.

Andersen, T., Elburg, M., Erambert, M., 2016. The miaskitic-to-agpaitic transition in peralkaline nepheline syenite (white foyaite) from the Pilanesberg Complex, South Africa. Chem. Geol. 455, 166–181.

Armbruster, T., Bonazzi, P., Akasaka, M., Bermanec, V., Chopin, C., Gieré, R., Heuss-Assbichler, S., Liebscher, A., Menchetti, S., Pan, Y., Pasero, M., 2006. Recommended nomenclature of epidote-group minerals. Eur. J. Mineral. 18, 551–567.

Aseri, A.A., Linnen, R.L., Che, X.D., Thibault, Y., Holtz, F., 2015. Effects of fluorine on the solubilities of Nb, Ta, Zr and Hf minerals in highly fluxed water-saturated haplogranitic melts. Ore Geol. Rev. 64, 736–746.

Bagiński, B., Zozulya, D., Macdonald, R., Kartashov, P.M., Dzierżanowski, P., 2016. Low-temperature hydrothermal alteration of a rare-metal rich quartz-epidote metasomatite from the El'ozero deposit, Kola Peninsula. Russia. Eur. J. Mineral. 28, 789–810. https://doi.org/10.1127/ejm/2016/0028-2552.

Balagansky, V.V., Myskova, T.A., Lvov, P.A., Larionov, A.N., Gorbunov, I.A., 2021. Neoarchean A-type acid metavolcanics in the Keivy Terrane, northeastern Fennoscandian Shield: geochemistry, age, and origin. Lithos 380, 105899.

Ballouard, C., Massuyeau, M., Elburg, M.A., Tappe, S., Viljoen, F., Brandenburg, J.-T., 2020. The magmatic and magmatic-hydrothermal evolution of felsic igneous rocks as seen through Nb-Ta geochemical fractionation, with implications for the origins of rare-metal mineralizations. Earth-Sci. Rev. 203, 103115 https://doi.org/10.1016/j.earscirev.2020.103115.

Ballouard, C., Poujol, M., Boulvais, P., Branquet, Y., Tartèse, R., Vigneresse, J.-L., 2016. Nb-Ta fractionation in peraluminous granites: A marker of the magmatic-hydrothermal transition. Geology 44, 231–234. https://doi.org/10.1130/G37475.1.

Batieva, I.D., 1976. Petrology of Alkaline Granitoids of the Kola Peninsula. Nauka, St. Petersburg.

Bernau, R., Franz, G., 1987. Crystal chemistry and genesis of Nb-, V-, and Al-rich metamorphic titanite from Egypt and Greece. Can. Mineral. 25, 695–705.

Boily, M., Williams-Jones, A.E., 1994. The role of magmatic and hydrothermal processes in the chemical evolution of the Strange Lake plutonic complex. Québec-Labrador. Contrib. Mineral. Petrol. 118, 33–47.

Breiter, K., Škoda, R., 2017. Zircon and whole-rock Zr/Hf ratios as markers of the evolution of granitic magmas: Examples from the Teplice caldera (Czech Republic/Germany). Miner. Petrol. 111, 435–457. https://doi.org/10.1007/s00710-017-0509-z.

Broska, I., Harlov, D., Tropper, P., Siman, P., 2007. Formation of magmatic titanite and titanite-ilmenite phase relations during granite alteration in the Tribec Mountains, Western Carpathians, Slovakia. Lithos 95, 58–71.

Černý, P., Ercit, T.S., 1989. Mineralogy of niobium and tantalum: crystal chemical relationships, paragenetic aspects and their economic implications. In: Möller P, Černý P, Saupé F (eds) Lanthanides, tantalum and niobium. Springer, SGA Spec Pub 7, 27-79.

Černý, P., Ercit, T.S., 2005. The classification of granitic pegmatites revisited. Can. Mineral. 43, 2005–2026.

Černý, P., Novák, M., Chapman, R., 1995. The AI(Nb, Ta)Ti_2 substitution in titanite: the emergence of a new species? Mineral. Petrol. 52, 61–73.

Chakhmouradian, A.R., 2004. Crystal chemistry and paragenesis of compositionally unique (Al-, Fe-, Nb-, and Zr-rich) titanite from Afrikanda, Russia. Am. Mineral. 89, 1752–1762. https://doi. org/10.2138/am-2004-11-1222.

Chakrabarty, A., Mitchell, R.H., Ren, M., Pal, S., Sen, A.K., 2018. Nb–Zr–REE Re-Mobilization and Implications for Transitional Agpaitic Rock Formation: Insights from the Sushina Hill Complex. India. J. Petrol. 59, 1899–1938. https://doi.org/10.1093/petrology/egy084.

Charoy, B., Raimbault, L., 1994. Zr-rich, Th-rich, and REE-rich biotite differentiates in the A-type granite pluton of Suzhou (Eastern China) - the key role of fluorine. J. Petrol. 35, 919–962. https://doi.org/10.1093/petrology/35.4.919.

Chen, Y.-X., Zheng, Y.-F., 2015. Extreme Nb/Ta fractionation in metamorphic titanite from ultrahigh-pressure metagranite. Geochim. Cosmochim. Acta 150, 53–73.

Clark, A.M., 1974. A tantalum-rich variety of sphene. Mineral. Mag. 39, 605–607.

Daly, S.J., Mitrofanov, F.P., Morozova, L.N., 1993. Late Archaean Sm-Nd model ages from the Voche-Lambina area: implications for the age distribution of Archaean crust in the Kola Peninsula. Russia. Prec. Res. 64, 189–195. https://doi.org/10.1016/0301-9268(93)90075-d.

Deer, W.A., Howie, R.A., Zussman, J., 1982. Rock-Forming Minerals. Orthosilicates, vol. 1A. Longman, London.

Gao, X.Y., Zheng, Y.F., Chen, Y.X., Guo, J.L., 2012. Geochemical and U-Pb age constraints on the occurrence of polygenetic titanites in UHP metagranite in the Dabie orogen. Lithos 136–139, 93–108.

Gieré, R., 1992. Compositional variation of metasomatic titanite from Adamello (Italy). Swiss Bull. Mineral. Petrol. 72, 167–177.

Gieré, R., Sorensen, S.S., 2004. Allanite and other REE-rich epidote group minerals. Rev. Mineral. Geochem. 56, 431–493.

Gerasimovskiy, V.I., Nesmeyanova, L.I., Kakhana, M.M., Khazizova, V.D., 1972. Trends in the Zr and Hf distributions for lavas of the East African Rift zones. Geochemistry 12, 1078–1086.

Gramaccioli, C.M., Diella, V., Demartin, F., 1999. The role of fluoride complexes in REE geochemistry and the importance of 4f electrons: some examples in minerals. Eur. J. Mineral. 11, 983–992.

Groat, L.A., Carter, R.T., Hawthorne, F.C., Ercit, T.S., 1985. Tantalian niobian titanite from the Irgon claim, southeastern Manitoba. Can. Mineral. 23, 569–571.

Gros, K., Słaby, E., Jokubauskas, P., Sláma, J., Kozub-Budzyń, G., 2020. Allanite Geochemical Response to Hydrothermal Alteration by Alkaline, Low-Temperature Fluids. Minerals 10, 392; 10.3390/min10050392.

Gros, K., Słaby, E., Birski, Ł., Kozub-Budzyń, G., Sláma, J., 2020b. Geochemical evolution of a composite pluton: insight from major and trace element chemistry of titanite. Mineral. Petrol. 114, 375–401.

Hanchar, J.M., Hoskin, P.W.O. (Eds) Zircon. Reviews in Mineralogy and Geochemistry. Washington, 2003. 500 p.

Huhma, H., Kontinen, A., Mikkola, P., Halkoaho, T., Hokkanen, T., Hölttä, P., Juopperi, H., Konnunaho, J., Luukkonen, E., Mutanen, T., Peltonen, P., Pietikäinen, K., Pulkkinen, A., 2012. Nd isotopic evidence for Archaean crustal growth in Finland. Geol. Surv. Finland Spec. Paper 54, 176–213.

Jacobsen, M.I., Reeve, J., Koepke, S., Perera, N., 2007. Pegmatite mineralogy of Western Australia. Mineral. Rec. 38, 319.

Kalashnikov, A.O., Konopleva, N.G., Pakhomovsky, Y.A., Ivanyuk, G.Y., 2016. Rare earth deposits of the murmansk region, russia—a review. Econ. Geol. 111, 1529–1559. https://doi.org/10.2113/econgeo.111.7.1529.

Keppler, H., 1993. Influence of fluorine on the enrichment of high-field strength trace-elements in granitic rocks. Contrib. Mineral. Petrol. 114, 479–488. https://doi.org/10.1007/bf00321752.

Kontonikas-Charos, A., Ehrig, K., Cook, N.J., Ciobanu, C.L., 2019. Crystal chemistry of titanite from the Roxby Downs Granite, South Australia: insights into petrogenesis, subsolidus evolution and hydrothermal alteration. Contrib. Mineral. Petrol. 174, 59. https://doi.org/10.1007/s00410-019-1594-2.

Kosterin, A.V., 1959. On possible forms of transfer of rare-earth elements by hydrothermal solutions. Geokhimiya 4, 310–315.

Kropáč, K., Dolníček, Z., Uher, P., Buriánek, D., Safai, A., Urubek, T., 2020. Zirconian–niobian titanite and associated Zr-, Nb-, REE-rich accessory minerals: Products of hydrothermal overprint of leucocratic teschenites (Silesian Unit, Outer Western Carpathians, Czech Republic). Geologica Carpathica 71, 343–360. 10.31577/GeolCarp.71.4.4.

Kudryashov, N.M., Skublov, S.G., Galankina, O.L., Udoratina, O.V., Voloshin, A.V., 2020. Abnormally high-hafnium zircon from rare-metal pegmatites of the Vasin-Mylk

deposit (the northeastern part of the Kola Peninsula). Geochemistry 80, 125489. https://doi.org/10.1016/j.geoch.2018.12.001.
Kuz'menko M.V. Geochemistry of tantalum and genesis of endogenic tantalum ore deposits. Nauka, Moscow. 1978, 214p.
Li, L., Xiong, X.L., Liu, X.C., 2017. Nb/Ta fractionation by amphibole in hydrous basaltic systems: implications for arc magma evolution and continental crust formation. J. Petrol. 58, 3–28. https://doi.org/10.1093/petrology/egw070.
Liferovich, R.P., Mitchell, R.H., 2006a. Solid solutions of niobium in synthetic titanite. Can. Mineral. 44, 1089–1097.
Liferovich, R.P., Mitchell, R.H., 2006b. Tantalum-bearing titanite: synthesis and crystal structure data. Phys. Chem. Minerals 33, 73–83. https://doi.org/10.1007/s00269-006-0069-y.
Linnen, R.L., Keppler, H., 2002. Melt composition control of Zr/Hf fractionation in magmatic processes. Geochim. Cosmochim. Acta 66, 3293–3301.
Linnen, R.L., Samson, I.M., eds., 2005. Rare element geochemistry and mineral deposits. Geol. Assoc. Canada Short Course Notes, 17.
Linnen, R.L., Samson, I.M., Williams-Jones, A.E., Chakhmouradian, A.R., 2014. Geochemistry of the Rare-Earth Elements, Nb, Ta, Hf, and Zr Deposits, in: Treatise on Geochemistry, 2nd ed., pp. 543-568.
Lowery Claiborne, L., Miller, C.F., Walker, B.A., Wooden, J.L., Mazdab, F.K., Bea, F., 2006. Tracking magmatic processes through Zr/Hf ratios in rocks and Hf and Ti zoning in zircons: an example from the Spirit Mountain batholith. Nevada. Mineral. Mag. 70, 517–543. https://doi.org/10.1180/0026461067050348.
Lyalina, L.M., Zozulya, D.R., Bayanova, T.B., Selivanova, E.A., Savchenko, Ye. E., 2012. Genetic peculiarities of zircon from pegmatites of Neoarchean alkali granites of the Kola region. Zapiski RMO 5, 35–51.
Lyalina, L.M., Selivanova, E.A., Savchenko, Y.E., Zozulya, D.R., Kadyrova, G.I., 2014. Minerals of the gadolinite-(Y)-hingganite-(Y) series in the alkali granite pegmatites of the Kola Peninsula. Geol. Ore Depos. 56, 675–684.
Marks, M.A.W., Markl, G., 2017. A global review on agpaitic rocks. Earth-Sci. Rev. 173, 229–258.
Marks, M.A.W., Hettmann, K., Schilling, J., Frost, B.R., Markl, G., 2011. The mineralogical diversity of alkaline igneous rocks: critical factors for the transition from miaskitic to agpaitic phase assemblages. J. Petrol. 52, 439–455.
Merlet, C., 1994. An accurate computer correction program for quantitative electron probe microanalysis. Microchim. Acta 114, 363-376. doi.org/10.1007/BF01244563.
Mikhailova, J.A., Pakhomovsky, Ya.A., Ivanyuk, G.Yu, Bazai, A.V., Yakovenchuk, V.N., Elizarova, I.R., Kalashnikov, A.O., 2017. REE mineralogy and geochemistry of the Western Keivy peralkaline granite massif, Kola Peninsula, Russia. Ore Geol. Rev. 82, 181–197. https://doi.org/10.1016/J.Oregeorev.2016.11.006.
Mineev, D.A., 1963. Geochemical differentiation of rare-earth elements. Geokhimiya 12, 1082–1100.
Mineev, D.A., 1968. Geochemistry of apogranites and rare-metal metasomatites of Northwestern Tarbagatai. Nauka, Moscow.
Mitrofanov, F.P., Zozulya, D.R., Bayanova, T.B., Levkovich, N.V., 2000. The world's oldest anorogenic alkali granitic magmatism in the Keivy structure on the Baltic Shield. Dokl. Earth Sci. 374, 1145–1148.
Nakada, S., 1991. Magmatic processes in titanite-bearing dacites, central Andes of Chile and Bolivia. Am. Mineral. 76, 548–560.
Neves, J.C., Nunes, J.L., Sahama, T.G., 1974. High hafnium members of the zircon-hafnon series from the granite pegmatites of Zambezia, Mozambique. Contrib. Mineral. Petrol. 48, 73–80.
Orlandi, P., Pasero, M., 2006. Allanite-(La) from Buca della Vena mine, Apuan Alps, Italy, an epidote-group mineral. Can. Mineral. 44, 63–68.
Paul, B.J., Černý, P., Chapman, R., 1981. Niobian titanite from the Huron Claim pegmatite, southeastern Manitoba. Can. Mineral. 19, 549–552.
Petrik, L., Broska, I., Lipka, J., Siman, P., 1995. Granitoid allanite-(Ce) substitution relations, redox conditions and REE distribution (on an example of I-type granitoids, Western Carpathians, Slovakia). Geol. Carpathica 46, 79–94.
Piilonen, P.C., Lalonde, A.E., McDonald, A.M., Gault, R.A., Larsen, A.O., 2003. Insights into astrophyllite-group minerals. 1. Nomenclature, composition and development of a standardized general formula. Can. Mineral. 41, 1–26.
Seifert, W., Kramer, W., 2003. Accessory titanite: an important carrier of zirconium in lamprophyres. Lithos 71, 81–98.
Škoda, R., Cempirek, J., Filip, J., Novak, M., Veselovsky, F., Ctvrtlik, R., 2012. Allanite-(Nd), $CaNdAl_2Fe^{2+}(SiO_4)(Si_2O_7)O(OH)$, a new mineral from Askagen. Sweden. Am. Mineral. 97, 983–988.
Skosyreva, M.V., Solodov, N.A., 1983. Geochemistry and Minerageny of Zirconium and Hafnium. VINITI, Moscow, p. 212.
Słaby, E., Anczkiewicz, R., Gros, K., Simon, K., Kozub-Budzyń, G.A., Birski, L., Martin, H., Jayananda, M., Moyen, J.-F., Matyszczak, M., Koziarska, M., Deput, E., 2021. High-temperature fluids in granites during the Neoarchaean-Palaeoproterozoic transition: Insight from Closepet titanite chemistry and U-Pb dating (Dharwar craton, India). Lithos 386–387, 106039. https://doi.org/10.1016/j.lithos.2021.106039.
Smith, M.P., Henderson, P., Campbell, L.S., 2000. Fractionation of the REE during hydrothermal processes: Constraints from the Bayan Obo Fe-REE-Nb deposit, Inner Mongolia, China. Geochim. Cosmochim. Acta 64, 3141–3160.
Smith, M.P., Storey, C.D., Jeffries, T.E., Ryan, C., 2009. In situ U-Pb and trace element analysis of accessory minerals in the Kiruna District, Norrbotten, Sweden: new constraints on the timing and origin of mineralization. J. Petrol. 50, 2063–2094.
Smith, P.E., Tatsumoto, M., Farquhar, R., 1987. Zircon Lu–Hf systematics and evolution of the Archean crust in the southern Superior Province, Canada. Contrib. Mineral. Petrol. 97, 93–104.
Sørensen, H., 1997. The agpaitic rocks — an overview. Mineral. Mag. 61, 485–498.
Stepanov, A., Mavrogenes, J.A., Meffre, S., Davidson, P., 2014. The key role of mica during igneous concentration of tantalum: Contrib. to Mineral. Petrol. 2014, 167, 1–8. 10.1007/s00410-014-1009-3.
Sun, S.S., McDonough, W.F., 1989. Chemical and isotopic systematics of oceanic basalts: Implications for mantle composition and processes. Geol. Soc. Lond. Spec. Publ. 42, 313–345.
Taylor, R.P., Strong, D.F., Fryer, B.J., 1981. Volatile control of contrasting trace-element distributions in peralkaline granitic and volcanic-rocks. Contrib. Mineral. Petrol. 77, 267–271. https://doi.org/10.1007/bf00373542.
Tiepolo, M., Oberti, R., Vannucci, R., 2002. Trace-element incorporation in titanite: constraints from experimentally determined solid/liquid partition coefficients. Chem. Geol. 191, 105–119.
Verplanck, P.L., Van Gosen, B.S., Seal, R.R., McCafferty, A.E., 2014. A deposit model for carbonatite and peralkaline intrusion-related rare earth element deposits. U.S. Geol. Surv. Sci. Investigations Rep. 2010–5070-J, 58.
Vetrin, V.R., Rodionov, N.V., 2009. Geology and geochronology of Neoarchean anorogenic magmatism of the Keivy structure, Kola Peninsula. Petrology 17, 537–557.
Vlach, S.R.F., Gualda, G.A.R., 2007. Allanite and chevkinite in A-type granites and syenites of the Graciosa Province, southern Brazil. Lithos 97, 98–121.
Voloshin, A.V., Lyalina, L.M., Savchenko, E.E, Selivanova, E.A., 2005. Intragranite raremetal pegmatites in alkaline-granite formation of Kola Peninsula. Quartz-zircon pseudomorphs. Zapiski RMO 4, 98-108 (in Russian with English abstract).
Voloshin, A.V., Pakhomovskii, Ya.A., 1986. Minerals and Evolution of Mineral Formation in Amazonite Pegmatites of the Kola Peninsula. Nauka, Leningrad.
Vuorinen, J.H., Hålenius, U., 2005. Nb-, Zr- and LREE-rich titanite from the Alnö alkaline complex: Crystal chemistry and its importance as a petrogenetic indicator. Lithos 83, 128–142. https://doi.org/10.1016/j.lithos.2005.01.008.
Wang, X., Griffin, W.L., Chen, J., 2010. Hf contents and Zr/Hf ratios in granitic zircons. Geoch. J. 44, 65–72.
Woolley, A.R., Platt, R.G., Eby, N., 1992. Niobian titanite and eudialite from Ilomba nepheline syenite complex, north Malawi. Mineral. Mag. 56, 428–430. https://doi.org/10.1180/minmag. 1992.056.384.19.
Xiao, X., Zhou, T., White, N.C., Zhang, L., Fan, Y., Chen, X., 2020. Multiple generations of titanites and their geochemical characteristics record the magmatic-hydrothermal processes and timing of the Dongguashan porphyry-skarn Cu-Au system, Tongling district, Eastern China. Miner. Deposita 56, 363–380. https://doi.org/10.1007/s00126-020-00962-0.
Xie, L., Wang, R.-C., Che, X.-D., Huang, F.-F., Erdmann, S., Zhang, W.-L., 2016. Tracking magmatic and hydrothermal Nb–Ta–W–Sn fractionation using mineral textures and composition: A case study from the late Cretaceous Jiepailing ore district in the Nanling Range in South China. Ore Geol. Rev. 78, 300–321. https://doi.org/10.1016/j.oregeorev.2016.04.003.
Yin, R., Wang, R.C., Zhang, A.C., Hu, H., Zhu, J.C., Rao, C., Zhang, H., 2013. Extreme fractionation from zircon to hafnon in the Koktokay No. 1 granitic pegmatite, Altai, northwestern China. Amer. Mineral. 98, 1714–1724.
Zaraisky, G.P., Korzhinskaya, V., and Kotova, N., 2010. Experimental studies of Ta2O5 and columbite–tantalite solubility in fluoride solutions from 300 to 550°C and 50 to 100 Mpa. Mineral. Petrol. 99, 287–300. 10.1007 /s00710 -010-0112-z.
Zhu, Z.-Y., Wang, R.-C., Che, X.-D., Zhu, J.-C., Wei, X.-L., Huang, X.E., 2015. Magmatic–hydrothermal rare-element mineralization in the Songshugang granite (northeastern Jiangxi, China): Insights from an electron-microprobe study of Nb–Ta–Zr minerals. Ore Geol. Rev. 65, 749–760. https://doi.org/10.1016/j.oregeorev.2014.07.02.
Zozulya, D.R., Bayanova, T.B., Eby, G.N., 2005. Geology and age of the Late Archean Keivy alkaline province, Northeastern Baltic Shield. J. Geol. 113, 601–608. https://doi.org/10.1086/431912.
Zozulya, D., Lyalina, L., Macdonald, R., Bagiński, B., Savchenko, Y., Jokubauskas, P., 2019. Britholite group minerals from REE-rich lithologies of Keivy alkali granite—nepheline syenite complex, Kola Peninsula, NW Russia. Minerals 9, 732. https://doi.org/10.3390/min9120732.
Zozulya, D.R., Lyalina, L.M., Eby, N., Savchenko, Y.E., 2012. Ore geochemistry, zircon mineralogy, and genesis of the Sakharjok Y-Zr deposit, Kola Peninsula, Russia. Geol. Ore Depos. 54, 81–98. https://doi.org/10.1134/s1075701512020079.
Zozulya, D., Macdonald, R., Bagiński, B., 2020. REE fractionation during crystallization and alteration of fergusonite-(Y) from Zr-REE-Nb–rich late- to post-magmatic products of the Keivy alkali granite complex, NW Russia. Ore Geol. Rev. 125, 103693 https://doi.org/10.1016/j.oregeorev.2020.103693.